CHEMISTRY
A European Journal

Supporting Information

Deciphering the Influence of Meridional versus Facial Isomers in Spin Crossover Complexes

Timothée Lathion,[a] Laure Guénée,[b] Céline Besnard,[b] Azzedine Bousseksou,[c] and Claude Piguet*[a]

chem_201804161_sm_miscellaneous_information.pdf

Author Contributions

T.L. Conceptualization: Equal; Data curation: Equal; Investigation: Lead; Methodology: Equal
L.G. Data curation: Lead; Investigation: Lead
C.B. Data curation: Lead; Investigation: Lead; Visualization: Equal
A.B. Methodology: Equal; Resources: Supporting; Validation: Supporting.

Appendix 1: SCO behavior of $[Fe(L2a)_3](PF_6)_2$ (4) in the solid state.

X-ray diffraction powder diagrams were recorded in the 140 et 340 K range for $[Fe(\mathbf{L2a})_3](PF_6)_2$ (**4**) and $[Zn(\mathbf{L2a})_3](PF_6)_2$. The *a*, *b*, *c* and *β* parameters of the monoclinic unit cells were refined at each temperature with the help of the *Le Bail* method and the unit cell volumes were computed and plotted in Figure A1-1.

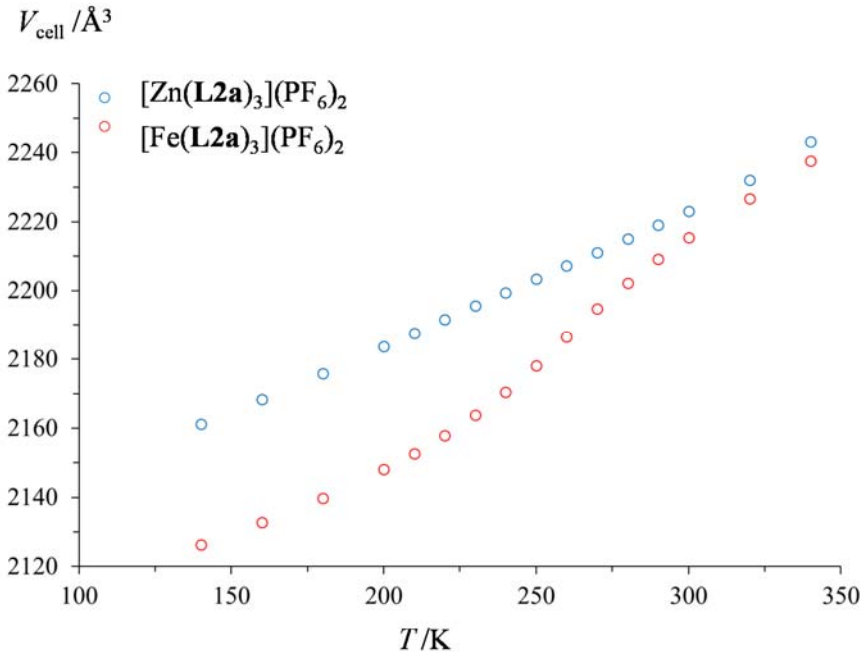

Figure A1-1. Temperature-dependence of the unit cell volumes in $[Zn(\mathbf{L2a})_3](PF_6)_2$ and $[Fe(\mathbf{L2a})_3](PF_6)_2$ (**4**).

The calculation of the isobaric thermal expansion coefficient at each temperature using Eq. (A1-1) lead to an almost constant value for $[Zn(\mathbf{L2a})_3](PF_6)_2$ (blue dots in Figure A1-2), a trend in line with standard thermal behaviors in absence of chemical transformations or phase transitions.

$$\alpha = \frac{1}{V} \cdot \frac{dV}{dT} \qquad \text{(A1-1)}$$

For $[Fe(\mathbf{L2a})_3](PF_6)_2$, the bell-shaped trace (red dots in Figure A1-2) points to an additional contribution to the volume expansion tentatively assigned to the operation of the spin crossover transition within this temperature range. (Eq. (A1-2)).

$$\alpha_{tot} = \alpha_{therm} + \alpha_{SCO} \qquad \text{(A1-2)}$$

Taking α_{therm} as the isobaric expansion of the analogous Zn^{II} complex, α_{SCO} is easily deduced and could be plotted as green dots in Figure A1-2.

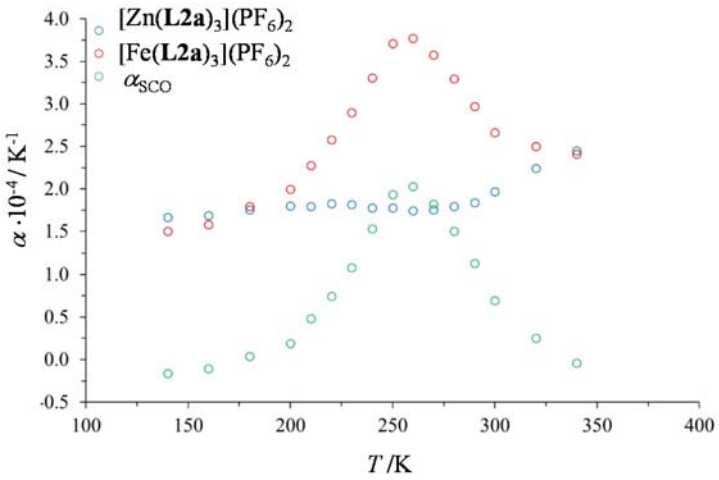

Figure A1-2 Temperature-dependence of the isobaric thermal expansion coefficients in [Zn(**L2a**)$_3$](PF$_6$)$_2$ (blue dots) and [Fe(**L2a**)$_3$](PF$_6$)$_2$ (red dots). $\alpha_{SCO} = \alpha_{tot} - \alpha_{therm} = \alpha_{Fe(\mathbf{L2a})_3} - \alpha_{Zn(\mathbf{L2a})_3}$ are shown as green dots (Eq. (A1-2)).

Finally the stepwise volume increases were obtained with Eqs (A1-3) and (A1-4) with the help of straightforward numerical integrations (Figure A1-3).

$$\Delta V_{therm}(T) = \int_{150}^{T} V(T) \cdot \alpha_{therm}(T) \cdot dT \qquad \text{(A1-3)}$$

$$\Delta V_{SCO}(T) = \int_{150}^{T} V(T) \cdot \alpha_{SCO}(T) \cdot dT \qquad \text{(A1-4)}$$

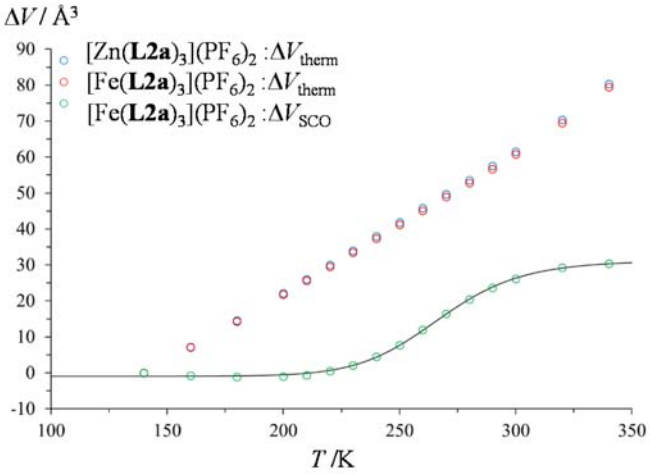

Figure A1-3. Temperature-dependence of the volume increases in [Zn(**L2a**)$_3$](PF$_6$)$_2$ (blue dots) and [Fe(**L2a**)$_3$](PF$_6$)$_2$ (red dots for thermal expansion, green dots for SCO expansion). The fitted full trace refers to a Hill plot $\Delta V_{sco} = \Delta V_{ls} + (\Delta V_{hs} - \Delta V_{ls}) / \left(1 + (T_{1/2}/T)^{z}\right)$ with ΔV_{ls} = -1.0(2) Å^3, ΔV_{hs} = 31.2(4) Å^3, $T_{½}$ = 267.3(7) K and z = 15.0(5).

Appendix 2: $\chi_M T$ as a function of ΔHsco, ΔS_{SCO} and $x_{Fe(III)}$: mixture of high-spin and low spin Fe(II) complexes with Fe(III) contamination.

The general expression of the Curie law for a mixture containing high-spin and low spin complexes together with traces of Fe^{III} oxidation products is:

$$\chi_M T = x_{hs} \cdot \left(C_{hs} + T \cdot TIP_{hs}\right) + x_{ls} \cdot \left(C_{ls} + T \cdot TIP_{ls}\right) + x_{Fe(III)} \cdot C_{Fe(III)} \quad (2)$$

The introduction of the mass balance depicted in Eq. (A2-1) into Eq. (2) gives Eq. (A2-2)

$$x_{hs} + x_{ls} + x_{Fe(III)} = 1 \quad (A2\text{-}1)$$

$$\chi_M T = x_{ls} \cdot \left(C_{ls} - C_{hs} + T \cdot \left(TIP_{ls} - TIP_{hs}\right)\right) + x_{Fe(III)} \cdot \left(C_{Fe(III)} - C_{hs} - T \cdot TIP_{hs}\right) + C_{hs} + T \cdot TIP_{hs} \quad (A2\text{-}2)$$

Taking into account the spin crossover equilibria $K_{sco} = x_{hs}/x_{ls}$ provides

$$\chi_M T = \frac{1 - x_{Fe(III)}}{1 + K_{sco}} \cdot \left(C_{ls} - C_{hs} + T \cdot \left(TIP_{ls} - TIP_{hs}\right)\right) + x_{Fe(III)} \cdot \left(C_{Fe(III)} - C_{hs} - T \cdot TIP_{hs}\right) + C_{hs} + T \cdot TIP_{hs} \quad (A2\text{-}3)$$

Finally, the introduction of the van't Hoff relationship $\Delta H_{sco} - T\Delta S_{sco} = -RT \ln\left(K_{sco}\right)$ yields

$$\chi_M T = \frac{\left(1 - x_{Fe(III)}\right) \cdot \left(C_{ls} - C_{hs} + T \cdot \left(TIP_{ls} - TIP_{hs}\right)\right)}{1 + \exp\left(\frac{1}{R} \cdot \left(\Delta S_{sco} - \frac{\Delta H_{sco}}{T}\right)\right)} + C_{hs} + T \cdot TIP_{hs} + x_{Fe(III)} \cdot \left(C_{Fe(III)} - C_{hs} - T \cdot TIP_{hs}\right)$$

(A3-3)

Eq. (A3-3) was used for fitting $\chi_M T$ to the thermodynamic parameters ΔH_{SCO}, ΔS_{SCO}, and to the amount of traces of Fe^{III}.

Appendix 3: $\chi_M T$ as a function of ΔH_{SCO}, ΔS_{SCO} and $x_{Fe(III)}$: mixture of high-spin and low spin Fe(II) complexes existing as meridional and facial isomers with Fe(III) contamination.

For mononuclear homoleptic tris-diimine Fe(II) complexes existing as a mixture of meridional and facial isomers, each displaying specific thermodynamic spin state equilibria but analogous (*i*. *e*. taken as identical) Curie constants (C_{hs} and C_{ls}) and temperature-independent parameters (TIP_{hs} and TIP_{ls})**,** Eq. (2) transforms into

$$\chi_M T = \left(x_{hs}^{fac} + x_{hs}^{mer}\right)\cdot\left(C_{hs} + T\cdot TIP_{hs}\right) + \left(x_{ls}^{fac} + x_{ls}^{mer}\right)\cdot\left(C_{ls} + T\cdot TIP_{ls}\right) + x_{Fe(III)}\cdot C_{Fe(III)} \quad (17)$$

The various mole fractions are correlated by mass balance (Eq. (A3-1)) and by thermodynamic constants (Eqs A3-2-A3-4).

$$x_{hs}^{fac} + x_{ls}^{fac} + x_{hs}^{mer} + x_{ls}^{mer} + x_{Fe(III)} = 1 \quad (A3\text{-}1)$$

$$K_{mer\rightarrow fac}^{Fe,\mathbf{Lk}} = \frac{x_{ls}^{fac} + x_{hs}^{fac}}{x_{ls}^{mer} + x_{hs}^{mer}} \quad (A3\text{-}2)$$

$$K_{SCO}^{fac\text{-}Fe(\mathbf{Lk})_3} = \frac{x_{hs}^{fac}}{x_{ls}^{fac}} \quad (A3\text{-}3)$$

$$K_{SCO}^{mer\text{-}Fe(\mathbf{Lk})_3} = \frac{x_{hs}^{mer}}{x_{ls}^{mer}} \quad (A3\text{-}4)$$

Straightforward mathematical manipulations yield

$$x_{ls}^{mer} = \frac{1 - x_{Fe(III)}}{\left(1 + K_{mer\rightarrow fac}^{Fe,\mathbf{Lk}}\right)\left(1 + K_{SCO}^{mer\text{-}Fe(\mathbf{Lk})_3}\right)} \quad (A3\text{-}5)$$

$$x_{hs}^{mer} = \frac{K_{SCO}^{mer\text{-}Fe(\mathbf{Lk})_3}\left(1 - x_{Fe(III)}\right)}{\left(1 + K_{mer\rightarrow fac}^{Fe,\mathbf{Lk}}\right)\left(1 + K_{SCO}^{mer\text{-}Fe(\mathbf{Lk})_3}\right)} \quad (A3\text{-}6)$$

$$x_{ls}^{fac} = \frac{K_{mer\rightarrow fac}^{Fe,\mathbf{Lk}}\left(1 - x_{Fe(III)}\right)}{\left(1 + K_{mer\rightarrow fac}^{Fe,\mathbf{Lk}}\right)\left(1 + K_{SCO}^{fac\text{-}Fe(\mathbf{Lk})_3}\right)} \quad (A3\text{-}7)$$

$$x_{hs}^{fac} = \frac{K_{SCO}^{fac\text{-}Fe(\mathbf{Lk})_3}\cdot K_{mer\rightarrow fac}^{Fe,\mathbf{Lk}}\left(1 - x_{Fe(III)}\right)}{\left(1 + K_{mer\rightarrow fac}^{Fe,\mathbf{Lk}}\right)\left(1 + K_{SCO}^{fac\text{-}Fe(\mathbf{Lk})_3}\right)} \quad (A3\text{-}8)$$

Finally, the introduction of Eqs (A3-5)-(A3-8) into Eq. (17) gives

$$\chi_{\mathrm{M}}T = \left(\frac{K_{\mathrm{SCO}}^{fac\text{-}\mathrm{Fe}(\mathbf{L}\boldsymbol{k})_3} \cdot K_{mer\rightarrow fac}^{\mathrm{Fe},\mathbf{L}\boldsymbol{k}} \left(1 - x_{\mathrm{Fe(III)}}\right)}{\left(1 + K_{mer\rightarrow fac}^{\mathrm{Fe},\mathbf{L}\boldsymbol{k}}\right)\left(1 + K_{\mathrm{SCO}}^{fac\text{-}\mathrm{Fe}(\mathbf{L}\boldsymbol{k})_3}\right)} + \frac{K_{\mathrm{SCO}}^{mer\text{-}\mathrm{Fe}(\mathbf{L}\boldsymbol{k})_3} \left(1 - x_{\mathrm{Fe(III)}}\right)}{\left(1 + K_{mer\rightarrow fac}^{\mathrm{Fe},\mathbf{L}\boldsymbol{k}}\right)\left(1 + K_{\mathrm{SCO}}^{mer\text{-}\mathrm{Fe}(\mathbf{L}\boldsymbol{k})_3}\right)} \right) \cdot \left(C_{\mathrm{hs}} + T \cdot TIP_{\mathrm{hs}}\right) + \left(\frac{K_{mer\rightarrow fac}^{\mathrm{Fe},\mathbf{L}\boldsymbol{k}} \left(1 - x_{\mathrm{Fe(III)}}\right)}{\left(1 + K_{mer\rightarrow fac}^{\mathrm{Fe},\mathbf{L}\boldsymbol{k}}\right)\left(1 + K_{\mathrm{SCO}}^{fac\text{-}\mathrm{Fe}(\mathbf{L}\boldsymbol{k})_3}\right)} + \frac{1 - x_{\mathrm{Fe(III)}}}{\left(1 + K_{mer\rightarrow fac}^{\mathrm{Fe},\mathbf{L}\boldsymbol{k}}\right)\left(1 + K_{\mathrm{SCO}}^{mer\text{-}\mathrm{Fe}(\mathbf{L}\boldsymbol{k})_3}\right)} \right) \cdot \left(C_{\mathrm{ls}} + T \cdot TIP_{\mathrm{ls}}\right) + x_{\mathrm{Fe(III)}} \cdot C_{\mathrm{Fe(III)}} \quad \text{(A3-9)}$$

Eq. (A3-9) was used for the fits of $\chi_{\mathrm{M}}T$ products collected for $[\mathrm{Fe}(\mathbf{L}\boldsymbol{k})_3]^{2+}$ in acetonitrile (Figure 8) with the help of the van't Hoff laws collected in Eqs (A3-10)-(A3-11).

$$K_{mer\rightarrow fac}^{\mathrm{Fe},\mathbf{L}\boldsymbol{k}} = \exp\left(\frac{1}{R}\left(\Delta S_{mer\rightarrow fac}^{\mathrm{Fe},\mathbf{L}\boldsymbol{k}} - \frac{\Delta H_{mer\rightarrow fac}^{\mathrm{Fe},\mathbf{L}\boldsymbol{k}}}{T} \right) \right) \quad \text{(A3-10)}$$

$$K_{\mathrm{SCO}}^{fac\text{-}\mathrm{Fe}(\mathbf{L}\boldsymbol{k})_3} = \exp\left(\frac{1}{R}\left(\Delta S_{\mathrm{SCO}}^{fac\text{-}\mathrm{Fe}(\mathbf{L}\boldsymbol{k})_3} - \frac{\Delta H_{\mathrm{SCO}}^{fac\text{-}\mathrm{Fe}(\mathbf{L}\boldsymbol{k})_3}}{T} \right) \right) \quad \text{(A3-11)}$$

$$K_{\mathrm{SCO}}^{mer\text{-}\mathrm{Fe}(\mathbf{L}\boldsymbol{k})_3} = \exp\left(\frac{1}{R}\left(\Delta S_{\mathrm{SCO}}^{mer\text{-}\mathrm{Fe}(\mathbf{L}\boldsymbol{k})_3} - \frac{\Delta H_{\mathrm{SCO}}^{mer\text{-}\mathrm{Fe}(\mathbf{L}\boldsymbol{k})_3}}{T} \right) \right) \quad \text{(A3-12)}$$

$\Delta H_{mer\rightarrow fac}^{\mathrm{Fe},\mathbf{L}\boldsymbol{k}}$ and $\Delta S_{mer\rightarrow fac}^{\mathrm{Fe},\mathbf{L}\boldsymbol{k}}$ were taken from Table S13, $\Delta H_{\mathrm{SCO}}^{fac\text{-}\mathrm{Fe}(\mathbf{L}\boldsymbol{k})_3}$ and $\Delta S_{\mathrm{SCO}}^{fac\text{-}\mathrm{Fe}(\mathbf{L}\boldsymbol{k})_3}$ were taken for $[\mathrm{LaFe}(\mathbf{L5})_3]^{5+}$, respectively $[\mathrm{LaFe}(\mathbf{L6})_3]^{5+}$ (Table 3) for pyrazine (**L1**), respectively pyridine (**L2**) derivatives and $\Delta H_{\mathrm{SCO}}^{mer\text{-}\mathrm{Fe}(\mathbf{L}\boldsymbol{k})_3}$ and $\Delta S_{\mathrm{SCO}}^{mer\text{-}\mathrm{Fe}(\mathbf{L}\boldsymbol{k})_3}$ were obtained by non-linear least-square fitting processes.

Table S1 Elemental analyses for mononuclear Fe(II) complexes.

complexes		%C	%N	%N	M_W /g·mol^{-1}
[Fe(**L1a**)$_3$](CF$_3$SO$_3$)$_2$ m = 424 mg, η = 84 %	Calcd	47.96	3.53	16.37	1026.8
	Found	47.81	3.53	16.36	
	Deviation	0.15	0.00	0.01	
[Fe(**L1a**)$_3$](PF$_6$)$_2$ m = 408 mg, η = 82 %	Calcd	45.99	3.56	16.50	1018.6
	Found	46.07	3.63	16.56	
	Deviation	0.08	0.07	0.06	
[Fe(**L2a**)$_3$](CF$_3$SO$_3$)$_2$·0.57H$_2$O m = 424 mg, η = 85 %	Calcd	51.11	3.91	12.19	1034.1
	Found	51.07	4.00	12.27	
	Deviation	0.04	0.09	0.08	
[Fe(**L2a**)$_3$](PF$_6$)$_2$·0.89H$_2$O m = 312 mg, η = 63 %	Calcd	48.90	3.98	12.22	1031.6
	Found	48.83	3.83	12.24	
	Deviation	0.07	0.15	0.02	
[Fe(**L3**)$_3$](CF$_3$SO$_3$)$_2$·2.31H$_2$O m = 224 mg, η = 75 %	Calcd	49.61	4.13	11.83	1065.4
	Found	49.57	3.81	11.78	
	Deviation	0.04	0.32	0.05	
[Fe(**bipy**)$_3$](CF$_3$SO$_3$)$_2$ m = 237 mg, η = 79 %	Calcd	46.73	2.94	10.22	822.5
	Found	46.56	2.97	10.14	
	Deviation	0.17	0.03	0.08	
[Fe(**L4**)$_3$](CF$_3$SO$_3$)$_2$·0.31H$_2$O m = 189.2 mg, η = 62 %	Calcd	51.34	3.88	12.25	1029.4
	Found	51.18	3.72	12.33	
	Deviation	0.16	0.16	0.08	
[Fe(**L4**)$_3$](PF$_6$)$_2$·0.89(nBu)$_4$NPF$_6$ m = 65.7 mg, η = 59 %	Calcd	49.65	5.26	10.18	1360.4
	Found	51.44	5.18	11.66	
	Deviation	1.79	0.08	1.48	
[Fe(**L4**)$_3$](BF$_4$)$_2$·0.19H$_2$O m = 90.9 mg, η = 67 %	Calcd	55.88	4.40	13.96	902.7
	Found	56.34	4.55	13.51	
	Deviation	0.46	0.15	0.45	

Table S2 Elemental analyses for dinuclear LnFe(II) and LnZn(II) helicates.

complexes		%C	%N	%N	M_W /g·mol^{-1}
[LaFe(**L5**)$_3$](CF$_3$SO$_3$)$_5$·6.95H$_2$O *m* = 98 mg, *η* = 68 %	Calcd	44.94	4.10	12.45	
	Found	45.00	3.93	12.28	2699.3
	Deviation	0.06	0.09	0.17	
[LaFe(**L5**)$_3$](PF$_6$)$_5$·4.02H$_2$O *m* = 47 mg, *η* = 87 %	Calcd	43.91	3.99	12.80	
	Found	44.10	4.08	12.61	2626.0
	Deviation	0.19	0.09	0.19	
[LaFe(**L6**)$_3$](CF$_3$SO$_3$)$_5$·0.30MeCN·4.88H$_2$O *m* = 122 mg, *η* = 85 %	Calcd	47.03	4.14	11.17	
	Found	47.05	4.16	11.15	2671.3
	Deviation	0.02	0.02	0.02	
[LaFe(**L6**)$_3$](PF$_6$)$_5$·0.30MeCN·4.88H$_2$O *m* = 46 mg, *η* = 79 %	Calcd	46.43	3.98	11.65	
	Found	46.60	4.15	11.48	2587.2
	Deviation	0.03	0.17	0.17	
[LaFe(**L7**)$_3$](CF$_3$SO$_3$)$_5$·0.04MeCN·5.96H$_2$O *m* = 88 mg, *η* = 77 %	Calcd	46.64	4.18	11.00	
	Found	46.60	4.13	11.04	2680.1
	Deviation	0.04	0.15	0.04	
[EuFe(**L5**)$_3$](CF$_3$SO$_3$)$_5$·0.23MeCN·3.50H$_2$O *m* = 114 mg, *η* = 77 %	Calcd	45.82	3.93	12.76	
	Found	45.85	3.96	12.73	2659.6
	Deviation	0.03	0.03	0.03	
[EuFe(**L5**)$_3$](PF$_6$)$_5$·0.28MeCN·2.19H$_2$O *m* = 47 mg, *η* = 87 %	Calcd	44.31	3.90	12.99	
	Found	44.53	4.12	12.77	2617.5
	Deviation	0.20	0.22	0.22	
[EuFe(**L6**)$_3$](CF$_3$SO$_3$)$_5$·0.31MeCN·4.04H$_2$O *m* = 118 mg, *η* = 81 %	Calcd	47.07	4.08	11.18	
	Found	47.12	4.13	11.13	2669.6
	Deviation	0.05	0.05	0.05	
[EuFe(**L6**)$_3$](PF$_6$)$_5$·1.28H$_2$O *m* = 49 mg, *η* = 87 %	Calcd	45.97	3.96	11.37	
	Found	46.15	3.96	11.19	2686.7
	Deviation	0.18	0.00	0.18	
[EuFe(**L7**)$_3$](CF$_3$SO$_3$)$_5$·6.68H$_2$O *m* = 75 mg, *η* = 78 %	Calcd	46.19	4.19	10.88	
	Found	46.06	4.06	10.83	2704.4
	Deviation	0.13	0.13	0.05	
[LaZn(**L5**)$_3$](CF$_3$SO$_3$)$_5$·5.11H$_2$O *m* = 64 mg, *η* = 93 %	Calcd	45.34	4.00	12.56	
	Found	45.24	3.90	12.62	2675.57
	Deviation	0.10	0.10	0.06	

$[LaZn(\mathbf{L6})_3](CF_3SO_3)_5 \cdot 0.35MeCN \cdot 4.60H_2O$ m = 68 mg, η = 90 %	Calcd	46.96	4.11	11.17	
	Found	46.91	4.06	11.22	2677.80
	Deviation	0.05	0.05	0.05	
$[LaZn(\mathbf{L7})_3](CF_3SO_3)_5 \cdot 0.03MeCN \cdot 6.01H_2O$ m = 62 mg, η = 87 %	Calcd	46.46	4.16	10.95	
	Found	46.45	4.15	10.96	2690.04x
	Deviation	0.01	0.01	0.01	
$[EuZn(\mathbf{L5})_3](CF_3SO_3)_5 \cdot 0.09MeCN \cdot 4.77H_2O$ m = 66 mg, η = 88 %	Calcd	45.24	3.97	12.56	
	Found	45.19	3.92	12.61	2686.20
	Deviation	0.05	0.05	0.05	
$[EuZn(\mathbf{L6})_3](CF_3SO_3)_5 \cdot 2.57H_2O$ m = 66 mg, η = 90 %	Calcd	47.32	3.98	11.14	
	Found	47.19	3.85	11.06	2639.95
	Deviation	0.13	0.13	0.08	
$[EuZn(\mathbf{L7})_3](CF_3SO_3)_5 \cdot 3.95H_2O$ m = 63 mg, η = 86 %	Calcd	46.88	4.04	11.04	
	Found	46.95	4.11	10.96	2664.79
	Deviation	0.07	0.07	0.08	

Table S3. Crystal data and structure refinement for $[Fe(\mathbf{L2a})_3](PF_6)_2$ (**4**).

Empirical formula	C42 H39 F12 Fe N9 P2	
Formula weight	1015.61	
Temperature	180(2) K	
Wavelength	1.54184 Å	
Crystal system	Monoclinic	
Space group	P 1 2/n 1	
Unit cell dimensions	a = 13.3060(3) Å	α= 90°.
	b = 10.8573(3) Å	β= 91.9459(18)°.
	c = 14.7855(3) Å	γ = 90°.
Volume	2134.79(8) $Å^3$	
Z	2	
Density (calculated)	1.580 Mg/m^3	
Absorption coefficient	4.412 mm^{-1}	
F(000)	1036	
Crystal size	0.3448 x 0.2089 x 0.0406 mm^3	
Theta range for data collection	4.07 to 73.85°.	
Index ranges	-15<=h<=16, -12<=k<=12, -18<=l<=18	
Reflections collected	16971	
Independent reflections	4257 [R(int) = 0.0255]	
Completeness to theta = 67.50°	99.9 %	
Absorption correction	Analytical	
Max. and min. transmission	0.838 and 0.431	
Refinement method	Full-matrix least-squares on F^2	
Data / restraints / parameters	4257 / 45 / 371	
Goodness-of-fit on F^2	1.055	
Final R indices [I>2sigma(I)]	R1 = 0.0897, wR2 = 0.2600	
R indices (all data)	R1 = 0.0934, wR2 = 0.2659	
Largest diff. peak and hole	0.881 and -0.919 $e.Å^{-3}$	

Table S4. Crystal data and structure refinement for [Fe(**L4**)$_3$](ClO$_4$)$_2$·CH$_3$CN (**5**).

Empirical formula	C44 H42 Cl2 Fe N10 O8	
Formula weight	965.62	
Temperature	180.15 K	
Wavelength	1.54184 Å	
Crystal system	Triclinic	
Space group	P -1	
Unit cell dimensions	a = 7.9648(3) Å	α= 73.505(3)°.
	b = 13.3150(5) Å	β= 89.165(3)°.
	c = 22.1652(9) Å	γ = 76.463(3)°.
Volume	2187.89(15) Å^3	
Z	2	
Density (calculated)	1.466 Mg/m^3	
Absorption coefficient	4.445 mm^{-1}	
F(000)	1000	
Crystal size	0.383 x 0.167 x 0.03 mm^3	
Theta range for data collection	3.566 to 73.813°.	
Index ranges	-9<=h<=8, -15<=k<=16, -27<=l<=27	
Reflections collected	14586	
Independent reflections	8551 [R(int) = 0.0238]	
Completeness to theta = 67.500°	99.9 %	
Absorption correction	Analytical	
Max. and min. transmission	0.876 and 0.417	
Refinement method	Full-matrix least-squares on F^2	
Data / restraints / parameters	8551 / 0 / 593	
Goodness-of-fit on F^2	1.040	
Final R indices [I>2sigma(I)]	R1 = 0.0736, wR2 = 0.2032	
R indices (all data)	R1 = 0.0814, wR2 = 0.2111	
Extinction coefficient	n/a	
Largest diff. peak and hole	1.386 and -0.553 e.Å^{-3}	

Table S5. Crystal data and structure refinement for [LaFe(**L5**)$_3$](ClO$_4$)$_5$·5CH$_3$CN (**6**).

Empirical formula	C106 H111 Cl5 Fe La N29 O23	
Formula weight	2531.24	
Temperature	180.00(10) K	
Wavelength	1.54184 Å	
Crystal system	Triclinic	
Space group	P -1	
Unit cell dimensions	a = 13.9174(2) Å	α= 82.7058(14)°.
	b = 15.7863(3) Å	β= 89.4978(14)°.
	c = 29.2215(5) Å	γ = 72.3254(16)°.
Volume	6064.50(19) Å^3	
Z	2	
Density (calculated)	1.386 Mg/m^3	
Absorption coefficient	5.313 mm^{-1}	
F(000)	2604	
Crystal size	0.255 x 0.154 x 0.089 mm^3	
Theta range for data collection	3.051 to 74.130°.	
Index ranges	-17<=h<=17, -19<=k<=18, -35<=l<=36	
Reflections collected	44738	
Independent reflections	23854 [R(int) = 0.0224]	
Completeness to theta = 67.500°	100.0 %	
Absorption correction	Analytical	
Max. and min. transmission	0.660 and 0.379	
Refinement method	Full-matrix least-squares on F^2	
Data / restraints / parameters	23854 / 2 / 1568	
Goodness-of-fit on F^2	1.038	
Final R indices [I>2sigma(I)]	R1 = 0.0554, wR2 = 0.1577	
R indices (all data)	R1 = 0.0594, wR2 = 0.1628	
Extinction coefficient	n/a	
Largest diff. peak and hole	1.492 and -0.982 e.Å^{-3}	

Table S6. Crystal data and structure refinement for [EuFe(**L5**)$_3$](ClO$_4$)$_5$·6CH$_3$CN (**7**).

Empirical formula	C108 H116 Cl5 Eu Fe N30 O24	
Formula weight	2603.36	
Temperature	180.00(10) K	
Wavelength	1.54184 Å	
Crystal system	Monoclinic	
Space group	P 1 21/c 1	
Unit cell dimensions	a = 21.7025(4) Å	α= 90°.
	b = 22.0035(5) Å	β= 98.868(2)°.
	c = 24.5216(4) Å	γ = 90°.
Volume	11569.8(4) Å^3	
Z	4	
Density (calculated)	1.495 Mg/m^3	
Absorption coefficient	6.620 mm^{-1}	
F(000)	5360	
Crystal size	0.793 x 0.055 x 0.046 mm^3	
Theta range for data collection	3.233 to 73.772°.	
Index ranges	-26<=h<=26, -22<=k<=27, -30<=l<=23	
Reflections collected	45660	
Independent reflections	22795 [R(int) = 0.0412]	
Completeness to theta = 67.500°	99.9 %	
Absorption correction	Analytical	
Max. and min. transmission	0.757 and 0.161	
Refinement method	Full-matrix least-squares on F^2	
Data / restraints / parameters	22795 / 11 / 1529	
Goodness-of-fit on F^2	1.024	
Final R indices [I>2sigma(I)]	R1 = 0.0572, wR2 = 0.1463	
R indices (all data)	R1 = 0.0763, wR2 = 0.1589	
Extinction coefficient	n/a	
Largest diff. peak and hole	1.482 and -1.249 e.Å^{-3}	

Table S7. Crystal data and structure refinement for [EuFe(**L6**)$_3$](CF$_3$SO$_3$)$_5$·2.5CH$_3$CN ·(CH$_3$)$_3$C(OCH$_3$) (**8**).

Empirical formula	C114 H118.50 Eu F15 Fe N23.50 O19 S5	
Formula weight	2774.93	
Temperature	180.01(10) K	
Wavelength	1.54184 Å	
Crystal system	Monoclinic	
Space group	C 2/c	
Unit cell dimensions	a = 57.7611(18) Å	α= 90°.
	b = 21.8156(6) Å	β= 99.735(3)°.
	c = 22.8883(7) Å	γ = 90°.
Volume	28426.1(15) Å^3	
Z	8	
Density (calculated)	1.297 Mg/m^3	
Absorption coefficient	5.361 mm^{-1}	
F(000)	11384	
Crystal size	0.208 x 0.188 x 0.074 mm^3	
Theta range for data collection	3.087 to 73.694°.	
Index ranges	-71<=h<=69, -26<=k<=16, -26<=l<=28	
Reflections collected	54948	
Independent reflections	27886 [R(int) = 0.0412]	
Completeness to theta = 67.500°	99.8 %	
Absorption correction	Analytical	
Max. and min. transmission	0.696 and 0.393	
Refinement method	Full-matrix least-squares on F^2	
Data / restraints / parameters	27886 / 96 / 1643	
Goodness-of-fit on F^2	1.021	
Final R indices [I>2sigma(I)]	R1 = 0.0741, wR2 = 0.2093	
R indices (all data)	R1 = 0.0935, wR2 = 0.2318	
Extinction coefficient	n/a	
Largest diff. peak and hole	1.391 and -0.908 e.Å^{-3}	

Table S8. Crystal data and structure refinement for {[LaFe(**L7**)$_3$](ClO$_4$)$_5$}$_2$·6CH$_3$CN·1.5H$_2$O (**9**).

Empirical formula	C210 H219 Cl10 Fe2 La2 N48 O47.50	
Formula weight	4919.34	
Temperature	180.00(10) K	
Wavelength	1.54184 Å	
Crystal system	Monoclinic	
Space group	P 1 21/c 1	
Unit cell dimensions	a = 30.9210(5) Å	α= 90°.
	b = 22.6412(3) Å	β= 94.890(2)°.
	c = 32.7303(4) Å	γ = 90°.
Volume	22830.7(6) Å^3	
Z	4	
Density (calculated)	1.431 Mg/m^3	
Absorption coefficient	5.620 mm^{-1}	
F(000)	10124	
Crystal size	0.392 x 0.149 x 0.041 mm^3	
Theta range for data collection	3.340 to 73.691°.	
Index ranges	-33<=h<=38, -27<=k<=16, -38<=l<=39	
Reflections collected	84627	
Independent reflections	44750 [R(int) = 0.0289]	
Completeness to theta = 67.500°	99.7 %	
Absorption correction	Analytical	
Max. and min. transmission	0.820 and 0.302	
Refinement method	Full-matrix least-squares on F^2	
Data / restraints / parameters	44750 / 21 / 2908	
Goodness-of-fit on F^2	1.022	
Final R indices [I>2sigma(I)]	R1 = 0.0601, wR2 = 0.1703	
R indices (all data)	R1 = 0.0790, wR2 = 0.1882	
Extinction coefficient	n/a	
Largest diff. peak and hole	1.371 and -0.979 e.Å^{-3}	

Table S9. Crystal data and structure refinement for {[EuFe(**L7**)$_3$](CF$_3$SO$_3$)$_5$}$_2$·4CH$_3$CN ·3(CH$_3$)$_3$C(OCH$_3$) (**10**).

Empirical formula	C231 H246 Eu2 F30 Fe2 N46 O39 S10	
Chemical formula moiety	2($C_{99}H_{99}Eu_1Fe_1N_{21}O_3$), 10($CF_3O_3S$), 4($C_2H_3N$), 3($C_5H_{12}O$)	
Formula weight	5596.94	
Temperature	180.00(10) K	
Wavelength	1.54184 Å	
Crystal system	Monoclinic	
Space group	P 21/c	
Unit cell dimensions	a = 28.3407(2) Å	α= 90°.
	b = 45.1598(3) Å	β= 112.4256(9)°.
	c = 22.37082(19) Å	γ = 90°.
Volume	26466.3(4) Å^3	
Z	4	
Density (calculated)	1.405 Mg/m^3	
Absorption coefficient	5.764 mm^{-1}	
F(000)	11496	
Crystal size	0.298 x 0.257 x 0.151 mm^3	
Theta range for data collection	3.335 to 67.406°.	
Index ranges	-33<=h<=17, -50<=k<=54, -26<=l<=26	
Reflections collected	97840	
Independent reflections	47569 [R(int) = 0.0318]	
Completeness to theta = 67.406°	99.9 %	
Absorption correction	Analytical	
Max. and min. transmission	0.566 and 0.347	
Refinement method	Full-matrix least-squares on F^2	
Data / restraints / parameters	47569 / 36 / 3194	
Goodness-of-fit on F^2	1.021	
Final R indices [I>2sigma(I)]	R1 = 0.0677, wR2 = 0.1980	
R indices (all data)	R1 = 0.0773, wR2 = 0.2103	
Extinction coefficient	n/a	
Largest diff. peak and hole	2.723 and -0.895 e.Å^{-3}	

Table S10. Crystal data and structure refinement for $[LuFe(\mathbf{L7})_3](CF_3SO_3)_5 \cdot 2CH_3CN$ (**11**).

Empirical formula	C108 H105 F15 Fe Lu N23 O18 S5	
Formula weight	2689.26	
Temperature	180.01(10) K	
Wavelength	1.54184 Å	
Crystal system	Triclinic	
Space group	P -1	
Unit cell dimensions	a = 15.1428(3) Å	α= 89.037(2)°.
	b = 18.9756(4) Å	β= 89.004(2)°.
	c = 22.6727(5) Å	γ = 68.864(2)°.
Volume	6075.3(2) $Å^3$	
Z	2	
Density (calculated)	1.470 Mg/m^3	
Absorption coefficient	4.100 mm^{-1}	
F(000)	2740	
Crystal size	0.276 x 0.161 x 0.04 mm^3	
Theta range for data collection	3.129 to 73.581°.	
Index ranges	-18<=h<=18, -23<=k<=15, -28<=l<=26	
Reflections collected	40621	
Independent reflections	22745 [R(int) = 0.0574]	
Completeness to theta = 67.500°	95.2 %	
Absorption correction	Semi-empirical from equivalents	
Max. and min. transmission	1.00000 and 0.52157	
Refinement method	Full-matrix least-squares on F^2	
Data / restraints / parameters	22745 / 0 / 1584	
Goodness-of-fit on F^2	1.043	
Final R indices [I>2sigma(I)]	R1 = 0.0634, wR2 = 0.1815	
R indices (all data)	R1 = 0.0738, wR2 = 0.1900	
Extinction coefficient	n/a	
Largest diff. peak and hole	1.967 and -1.680 $e.Å^{-3}$	

Table S11. Interatomic distances $d_{Ln\text{-}O}$ and $d_{Ln\text{-}N}$ recorded in the dinuclear helicates **6-11** in the solid state at 180 K.

complexe	$d_{Ln(III)-O}$ /Å	$d_{Ln(III)-N(bz)}$ [a] /Å	$d_{Ln(III)-N(py)}$ [a] /Å	Reference
$[EuZn(\mathbf{L5})_3]^{5+}$	2.40(2)	2.58(2)	2.61(3)	[15]
$[LaFe(\mathbf{L5})_3]^{5+}$	2.47(2)	2.68(3)	2.72(2)	This work
$[EuFe(\mathbf{L5})_3]^{5+}$	2.38(2)	2.57(3)	2.603(3)	This work
$[EuZn(\mathbf{L6})_3]^{5+}$	2.38(2)	2.57(4)	2.60(5)	[18a]
$[LaFe(\mathbf{L6})_3]^{5+}$	2.49(2)	2.677(8)	2.64(5)	[18b]
$[EuFe(\mathbf{L6})_3]^{5+}$	2.406(9)	2.575(9)	2.61(2)	This work
$[LaFe(\mathbf{L7})_3]^{5+}$	2.49(3)	2.69(1)	2.70(2)	This work
$[EuFe(\mathbf{L7})_3]^{5+}$	2.405(8)	2.579(7)	2.60(1)	This work
$[LuFe(\mathbf{L7})_3]^{5+}$	2.31(3)	2.49(3)	2.52(2)	This work

[a] bz = benzimidazole, py = pyridine.

Table S12. Cumulative stability constants ($\log\left(\beta_{1,n}^{\mathrm{M,L}k}\right)$, Eqs 4-6), intrinsic affinities ($\Delta G^{\mathrm{M,L}k}$), global ($\Delta E^{\mathrm{L}k,\mathrm{L}k}$) and specific ($\Delta E_{i,j}^{\mathrm{L}k,\mathrm{L}k}$, Eqs (7-9)) interligand interactions (acetonitrile 298 K).

Ligand	**L1a**		**L1b**		**L2a**		**L2b**	
Metal	Fe	Zn	Fe	Zn	Fe	Zn	Fe	Zn
$\log\left(\beta_{1,1}^{\mathrm{M,L}k}\right)$	6.045(9)	6.89(3)	5.175(5)	4.80(2)	7.0(1)	7.7(2)	5.44(1)	5.84(1)
$\log\left(\beta_{1,2}^{\mathrm{M,L}k}\right)$	11.49(2)	12.76(5)	9.94(1)	10.21(2)	14.7(2)	15.0(4)	12.00(3)	11.31(2)
$\log\left(\beta_{1,3}^{\mathrm{M,L}k}\right)$	16.88(2)	17.64(5)	15.10(1)	14.47(5)	21.9(4)	21.9(6)	17.49(4)	16.52(3)
$\Delta G^{\mathrm{M,L}k}$ kJ/mol	-25.9(8)	-31.1(3)	-21(1)	-21(1)	-32.9(8)	-35.8(2)	-25(2)	-25.1(4)
$\Delta E^{\mathrm{L}k,\mathrm{L}k}$ kJ/mol	-2.7(9)	1.1(4)	-4(1)	-3(2)	-5(1)	-2.5(3)	-5(2)	-2.9(4)
$\Delta E_{\mathrm{trans}}^{\mathrm{L}k,\mathrm{L}k}$ kJ/mol	47(2)	40(13)	-	-	-10(15)	4(14)	-	-
$\Delta E_{\mathrm{cis,mer}}^{\mathrm{L}k,\mathrm{L}k}$ kJ/mol	-1.98(3)	2.41(5)	-	-	-6.09(8)	-2.1(6)	-	-
$\Delta E_{\mathrm{cis,fac}}^{\mathrm{L}k,\mathrm{L}k}$ kJ/mol	-2.89(3)	0.59(5)	-	-	-6.11(8)	-2.4(6)	-	-
Reference	This work	[15]	This work	[15]	This work	[15]	This work	[15]

Table S13. Enthalpic ($\Delta H^{\mathrm{M,L}k}_{mer\rightarrow fac}$) and entropic ($\Delta S^{\mathrm{M,L}k}_{mer\rightarrow fac}$) contributions to the isomerization equilibrium (10) in CD_3CN (M = Fe^{II}, Zn^{II} and **L*k*** = **L1a**, **L2a**).

complexe	$\Delta H^{\mathrm{M,L}k}_{mer\rightarrow fac}$ /kJ·mol^{-1}	$\Delta S^{\mathrm{M,L}k}_{mer\rightarrow fac}$ /J·mol^{-1}·K^{-1}	$T_{½}$ [a] /K	Reference
$[Fe(\mathbf{L1a})_3]^{2+}$	-5(1)	-26(4)	206(51)	This work
$[Zn(\mathbf{L1a})_3]^{2+}$	-4(1)	-16(4)	277(94)	[15]
$[Fe(\mathbf{L2a})_3]^{2+}$	-2.9(5)	-22(2)	134(24)	This work
$[Zn(\mathbf{L2a})_3]^{2+}$	-1.7(1)	-14.0(5)	125(10)	[15]
$[Co(\mathbf{L2a})_3]^{2+}$	0.6(3)	-10(1)	[b]	[c]

[a] $T_{½}$ is the temperature at which $x_{\mathrm{fac}} = x_{\mathrm{mer}} = 0.5$. [b] not accessible. [c] L. J. Charbonnière, A. F. Williams, U. Frey, A. E. Merbach, P. Kamalaprija and O. Schaad, *J. Amer. Chem. Soc.* **1997**, *119*, 2488-2496 and L. J. Charbonnière, A. F. Williams, C. Piguet, G. Bernardinelli, E. Rivara-Minten, *Chem. Eur. J.* **1998**, *4*, 485-493.

Table S14. Intrashell d-d transition energies of $[Ni(\mathbf{L}k)_3]^{2+}$ complexes (acetonitrile, 293 K).

Complexes	$^3T_{2g}(^3F)$/ cm^{-1}	$^1E_g(^1D)$ /cm^{-1}	$^3T_{1g}(^3F)$ /cm^{-1}	$^3T_{1g}(^3P)$ /cm^{-1}	reference
$[Ni(\mathbf{bipy})_3]^{2+}$	12699 (6.7)[a]	11274 (0.6)	19236 (10.8)	[b]	This work
$[Ni(\mathbf{L1a})_3]^{2+}$	11476 (5.6)	12831 (0.4)	18195 (11.0)	[b]	This work
$[Ni(\mathbf{L1b})_3]^{2+}$	11628 (4.8)	12772 (0.2)	18440 (7.4)	[b]	This work
$[Ni(\mathbf{L2a})_3]^{2+}$	11423 (5.8)	12885 (0.5)	18199 (9.2)	[b]	This work
$[Ni(\mathbf{L2b})_3]^{2+}$	11567 (5.0)	12789 (0.4)	18372 (6.9)	[b]	This work
$[Ni(\mathbf{L3})_3]^{2+}$	9644 (7.5)	12563 (0.4)	15946 (6.7)	[b]	This work
$[Ni(\mathbf{L4})_3]^{2+}$	10681 (4.9)	12467 (0.4)	17266 (7.0)	[b]	This work
$[Ni(CH_3CN)_6]^{2+}$	9922 (4.8)	13881 (0.5)	16479 (3.9)	26902 (6.2)	This work
$[Ni(NH_3)_6]^{2+}$	10730	[c]	17530	28110	[48]
$[Ni(H_2O)_6]^{2+}$	8580	[c]	14300	25370	[48]

[a] Molar absorption coefficient in M^{-1}cm^{-1} are given between parentheses. [b] Masqued by charge transfer bands. [c] Not reported in reference [48].

Table S15. ESI-MS spectra recorded for $[LnM(\mathbf{L}\boldsymbol{k})_3](CF_3SO_3)_5$ ($2\cdot10^{-3}$ M in CH_3CN, 298 K)

Cations	*m*/*z* exp.	*m*/*z* calc.	*I* /%
$[\mathbf{L6}(H)_2]^{2+}$	272.91	272.64	9
$[\mathbf{L6}(H)]^{+}$	544.59	544.28	18
$[La(\mathbf{L6})(Otf)]^{2+}$	415.87	415.82	35
$[Zn(\mathbf{L6})_2]^{2+}$	575.71	576.36	21
$[LaZn(\mathbf{L6})_3]^{5+}$	367.46	367.06	100
$[LaZn(\mathbf{L6})_3(Otf)]^{4+}$	496.27	496.09	94
$[LaZn(\mathbf{L6})_3(Otf)_2]^{3+}$	711.41	711.15	62
$[LaZn(\mathbf{L6})_3(Otf)_3]^{2+}$	1141.18	1141.25	8
$[LaZn(\mathbf{L6})_3(Otf)_4]^{+}$	2431.45	2431.56	0.1
$[\mathbf{L7}(H)_2]^{2+}$	272.94	272.64	8
$[\mathbf{L7}(H)]^{+}$	544.60	544.28	25
$[La(\mathbf{L7})(Otf)]^{2+}$	415.86	415.82	42
$[Zn(\mathbf{L7})_2]^{2+}$	575.73	576.36	29
$[LaZn(\mathbf{L7})_3]^{5+}$	367.47	367.06	92
$[LaZn(\mathbf{L7})_3(Otf)]^{4+}$	496.27	493.09	100
$[LaZn(\mathbf{L7})_3(Otf)_2]^{3+}$	711.42	711.15	79
$[LaZn(\mathbf{L7})_3(Otf)_3]^{2+}$	1141.18	1141.25	15
$[LaZn(\mathbf{L7})_3(Otf)_4]^{+}$	2432.03	2431.56	0.2
$[\mathbf{L5}(H)_2]^{2+}$	273.41	273.14	18
$[\mathbf{L5}(H)]^{+}$	545.60	545.28	9
$[La(\mathbf{L5})(Otf)]^{2+}$	416.53	416.31	59
$[Zn(\mathbf{L5})_2]^{2+}$	575.74	577.34	26
$[LaZn(\mathbf{L5})_3]^{5+}$	367.69	367.65	100
$[LaZn(\mathbf{L5})_3(Otf)]^{4+}$	497.11	496.84	71
$[LaZn(\mathbf{L5})_3(Otf)_2]^{3+}$	712.19	712.13	56
$[LaZn(\mathbf{L5})_3(Otf)_3]^{2+}$	1142.60	1142.73	10
$[LaZn(\mathbf{L5})_3(OTf)_4]^{+}$	2436.10	2434.53	0.1

$[LaFe(\mathbf{L6})_3]^{5+}$	365.66	365.15	100
$[La(\mathbf{L6})(Otf)]^{2+}$	415.91	415.82	12
$[LaFe(\mathbf{L6})_3(Otf)]^{4+}$	493.92	493.70	88
$[\mathbf{L6}(H)]^{+}$	544.59 [a]	544.68	12
$[Fe(\mathbf{L6})_2]^{5+}$	571.58	571.58	22
$[LaFe(\mathbf{L6})_3(Otf)_2]^{3+}$	708.16	707.96	82
$[Fe(\mathbf{L6})_3]^{2+}$	843.79	843.42	6
$[LaFe(\mathbf{L6})_3(Otf)_3]^{2+}$	1136.26	1136.47	12
$[\mathbf{L7}(H)_2]^{2+}$	272.95	272.84	5
$[LaFe(\mathbf{L7})_3]^{5+}$	365.66	365.15	64
$[LaFe(\mathbf{L7})_3(Otf)]^{4+}$	493.91	493.70	100
$[\mathbf{L7}(H)]^{+}$	544.59	544.68	9
$[LaFe(\mathbf{L7})_3(Otf)_2]^{3+}$	708.13	707.96	45
$[LaFe(\mathbf{L7})_3(Of)_3]^{2+}$	1136.83	1136.47	14
$[\mathbf{L5}(H)_2]^{2+}$	273.37	273.33	7
$[LaFe(\mathbf{L5})_3]^{5+}$	366.18	365.74	100
$[LaFe(\mathbf{L5})_3(Otf)]^{4+}$	494.74	494.44	93
$[\mathbf{L5}(H)]^{+}$	545.57	545.66	18
$[Fe(\mathbf{L8})_2]^{2+}$	573.21	572.57	14
$[LaFe(\mathbf{L5})_3(Otf)_2]^{3+}$	709.35	708.95	64
$[Fe(\mathbf{L5})_3]^{2+}$	845.05	844.90	7
$[LaFe(\mathbf{L5})_3(Otf)_3]^{2+}$	1137.95	1137.96	11

Table S16. Thermodynamic parameters obtained by non-linear fits using Eq. (17) for the $\chi_M T$ versus T plots recorded for the homoleptic $[Fe(\mathbf{Lk})_3]X_2$ complexes in solution (CD_3CN) using various helicates as model for *fac*-$[Fe(\mathbf{L1a})_3]^{2+}$.

mer-$[Fe(\mathbf{L1a})_3]X_2$ *X*	model [a] $[MFe(\mathbf{L5})_3]^{5+}$ *M*	ΔH_{sco} /kJ·mol^{-1}	ΔS_{sco} /J·mol^{-1}·K^{-1}	$T_{½}$ /K	$x_{Fe(III)}$ /%	*AF* [b]
Otf^-	La(III)	35.9(6)	106(2)	339(8)	3.3(1)	$1.04\cdot10^{-2}$
Otf^-	Y(III)	35.9(5)	106(2)	340(7)	3.3(1)	$1.01\cdot10^{-2}$
Otf^-	Ca(II)	35.8(5)	105(2)	340(7)	3.3(1)	$1.01\cdot10^{-2}$
PF_6^-	La(III)	35.9(3)	104.1(9)	345(4)	0.00(7)	$5.13\cdot10^{-3}$
PF_6^-	Y(III)	36.0(3)	104(1)	346(5)	0.00(7)	$5.34\cdot10^{-3}$
PF_6^-	Ca(II)	35.9(3)	104(1)	346(4)	0.00(7)	$5.34\cdot10^{-3}$

[a] La(III): ΔH_{sco} = 37.9(5) kJ·mol^{-1}, ΔS_{sco} = 92(1) J·K^{-1}·mol^{-1}; Y(III): ΔH_{sco} = 34(2) kJ·mol^{-1}, ΔS_{sco} = 82(5) J·K^{-1}·mol^{-1}; Ca(II) ΔH_{sco} = 36.7(2) kJ·mol^{-1}, ΔS_{sco} = 90.2(6) J·K^{-1}·mol^{-1}. [b] $AF = (\Sigma(\chi_M T_{exp} - \chi_M T_{calc})^2/\Sigma(\chi_M T_{exp})^2)^{½}$

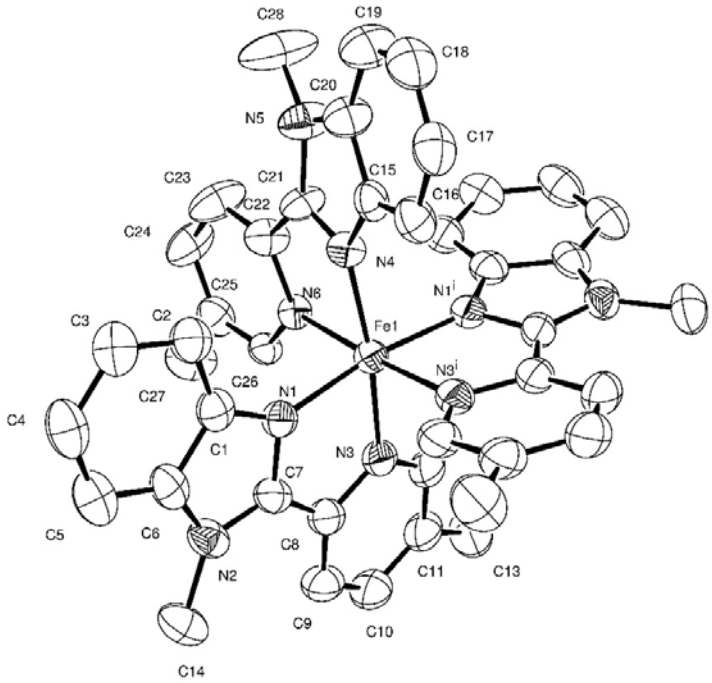

Figure S1. ORTEP view of $[Fe(\mathbf{L2a})_3]^{2+}$ in the crystal structure of $[Fe(\mathbf{L2a})_3](PF_6)_2$ (**4**) (ellipsoids are drawn at 50% probability) with numbering scheme. Hydrogen atoms and PF_6^- counter anions are omitted for clarity The complex (Fe atom) is lying on a twofold axis so that only one half of the complex is in the asymmetric unit. One ligand (N4-N6, passing through this 2-fold axis) is disordered by rotation and refined with occupancies fixed to 0.5 (only one configuration is shown).

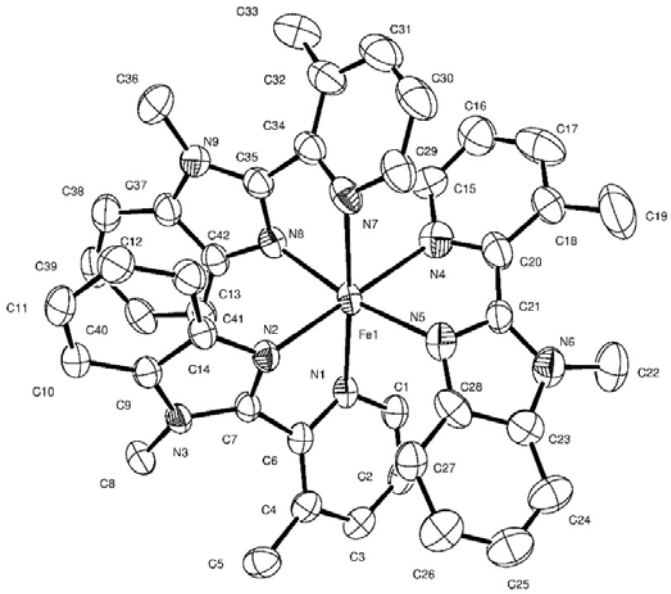

Figure S2. ORTEP view of $[Fe(\mathbf{L4})_3]^{2+}$ in the crystal structure of $[Fe(\mathbf{L4})_3](ClO_4)_2{\cdot}CH_3CN$ (**5**) (thermal ellipsoids are drawn at 50% probability level) with numbering scheme. Hydrogen atoms, ClO_4^- counter anions and solvent molecules are omitted for clarity.

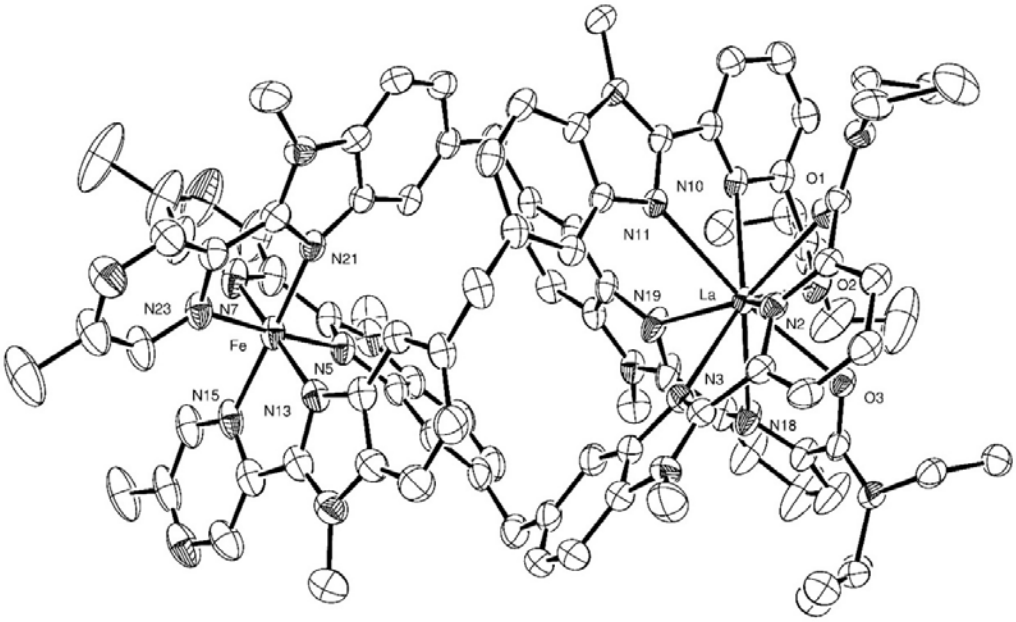

Figure S3. ORTEP view of HHH-[LaFe(**L5**)$_3$]$^{5+}$ in the crystal structure of [LaFe(**L5**)$_3$](ClO$_4$)$_5$·5CH$_3$CN (**6**) (thermal ellipsoids are drawn at 40% probability level) with numbering scheme of the coordination sites. Hydrogen atoms, ClO$_4^-$ counter anions and solvent molecules are omitted for clarity.

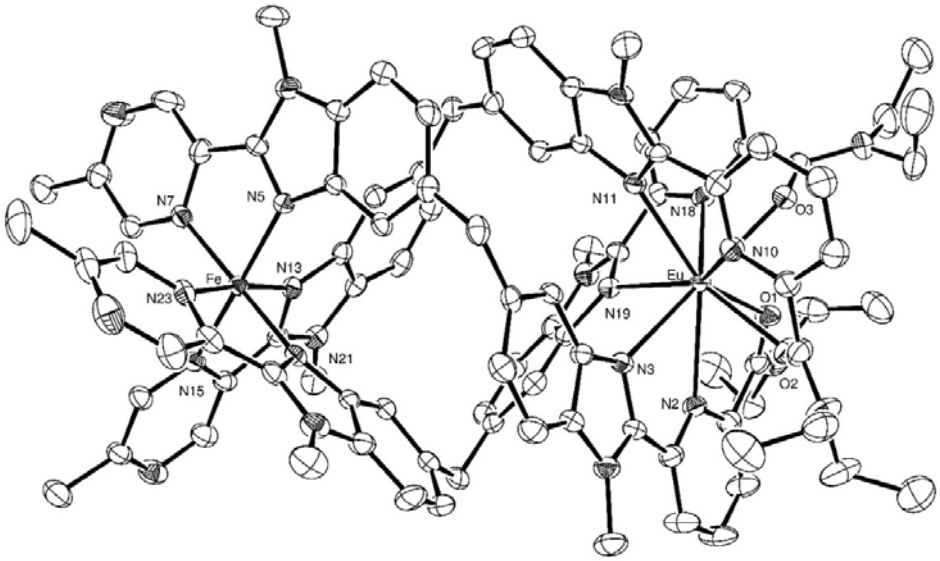

Figure S4. ORTEP view of HHH-[EuFe(**L5**)$_3$]$^{5+}$ in the crystal structure of [EuFe(**L5**)$_3$](ClO$_4$)$_5$·6CH$_3$CN **(7)** (thermal ellipsoids are drawn at 40% probability level) with numbering scheme. Hydrogen atoms, ClO$_4^-$ counter anions and solvent molecules are omitted for clarity.

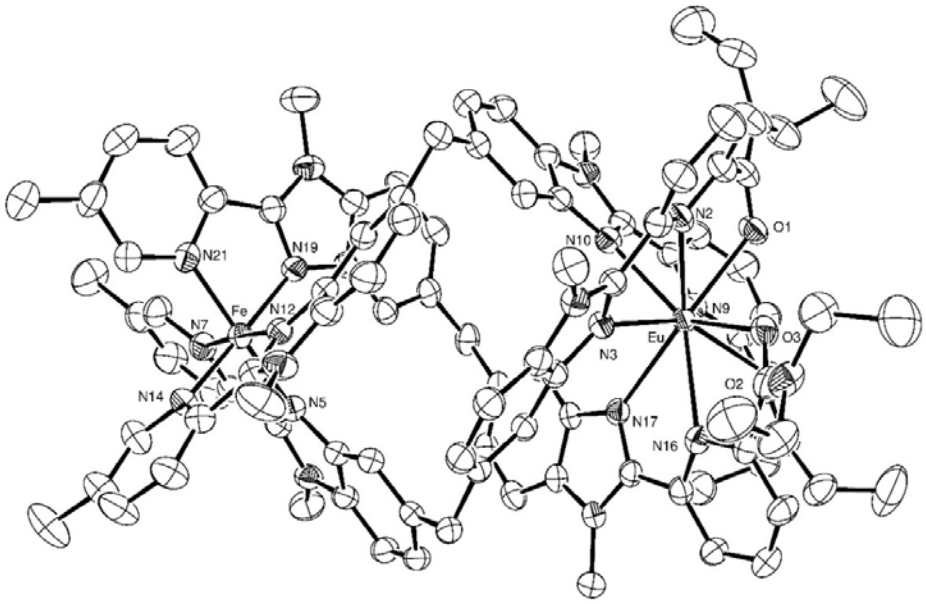

Figure S5. ORTEP view of HHH-[EuFe(**L6**)$_3$]$^{5+}$ in the crystal structure of [EuFe(**L6**)$_3$](CF$_3$SO$_3$)$_5$·2.5CH$_3$CN·(CH$_3$)$_3$C(OCH$_3$) (**8**) (thermal ellipsoids are drawn at 35% probability level) with numbering scheme. Hydrogen atoms, CF$_3$SO$_3^-$ counter anions and solvent molecules are omitted for clarity.

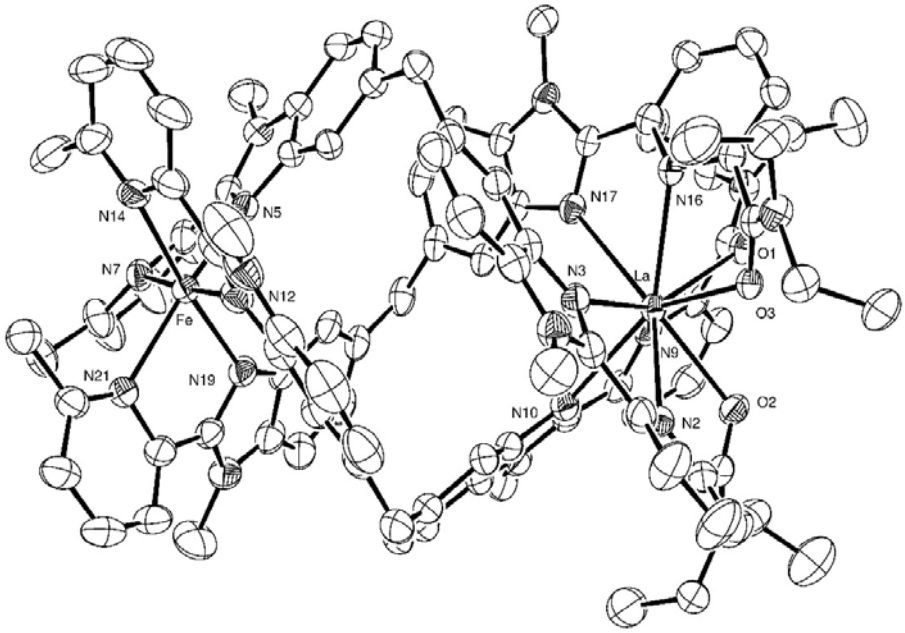

Figure S6. ORTEP view of HHH-[LaFe(**L7**)$_3$]$^{5+}$ in the crystal structure of {[LaFe(**L7**)$_3$](ClO$_4$)$_5$}$_2$·6CH$_3$CN·1.5H$_2$O (**9**) (thermal ellipsoids are drawn at 35% probability level) with numbering scheme. Only one of the two independent complex in the structure is shown. Hydrogen atoms, ClO$_4^-$ counter anions and solvent molecules are omitted for clarity.

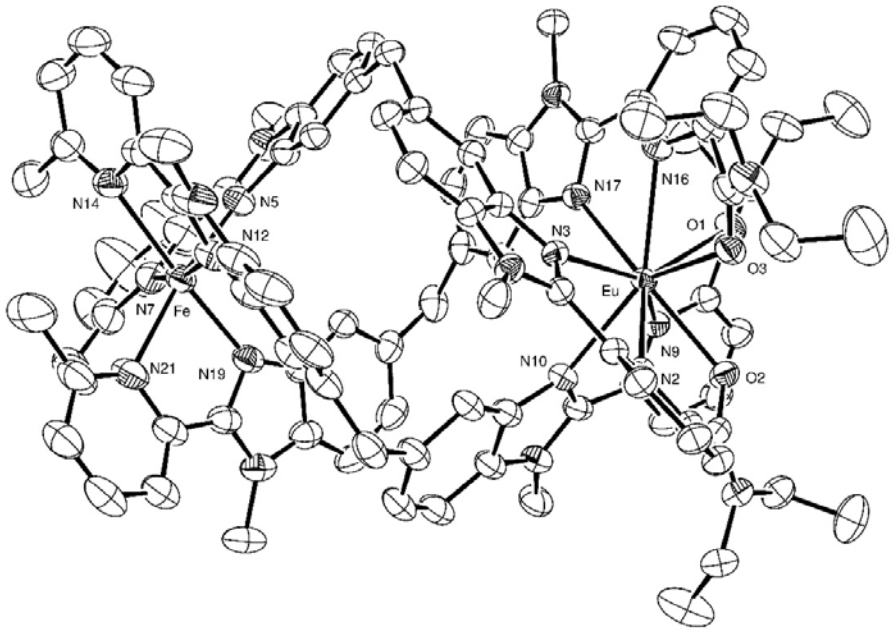

Figure S7. ORTEP view of HHH-[EuFe(**L7**)$_3$]$^{5+}$ in the crystal structure of {[EuFe(**L7**)$_3$](CF$_3$SO$_3$)$_5$}$_2$·4CH$_3$CN·3(CH$_3$)$_3$C(OCH$_3$) (**10**) (thermal ellipsoids are drawn at 35% probability level) with numbering scheme. Only one of the two independent complex in the structure is shown. Hydrogen atoms, $CF_3SO_3^-$ counter anions and solvent molecules are omitted for clarity.

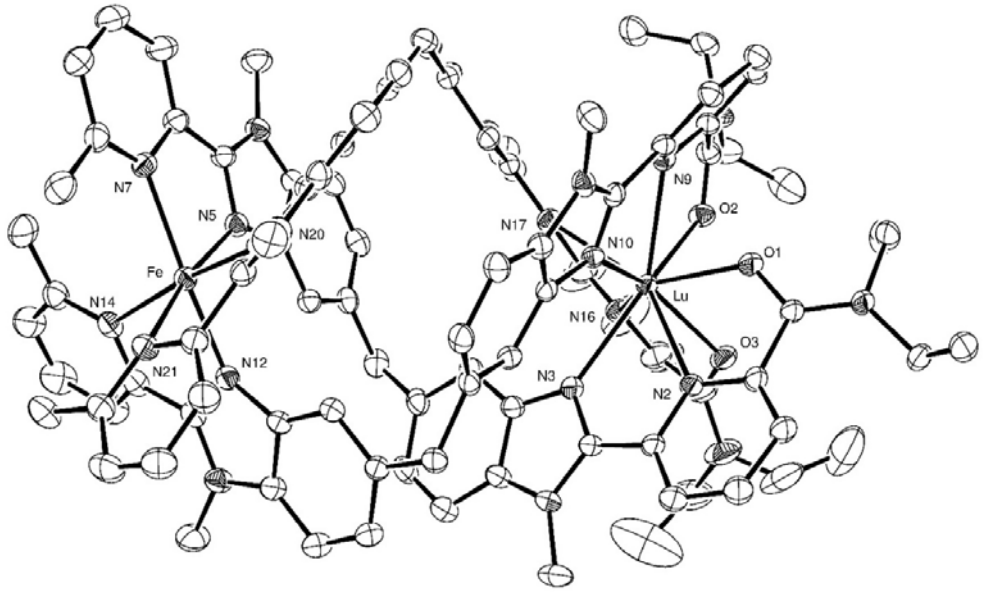

Figure S8. ORTEP view of HHH-[LuFe(**L7**)$_3$]$^{5+}$ in the crystal structure of [LuFe(**L7**)$_3$](CF$_3$SO$_3$)$_5$·2CH$_3$CN (**11**) (thermal ellipsoids are drawn at 35% probability level) with numbering scheme. Only one of the two independent complex in the structure is shown. Hydrogen atoms, $CF_3SO_3^-$ counter anions and solvent molecules are omitted for clarity.

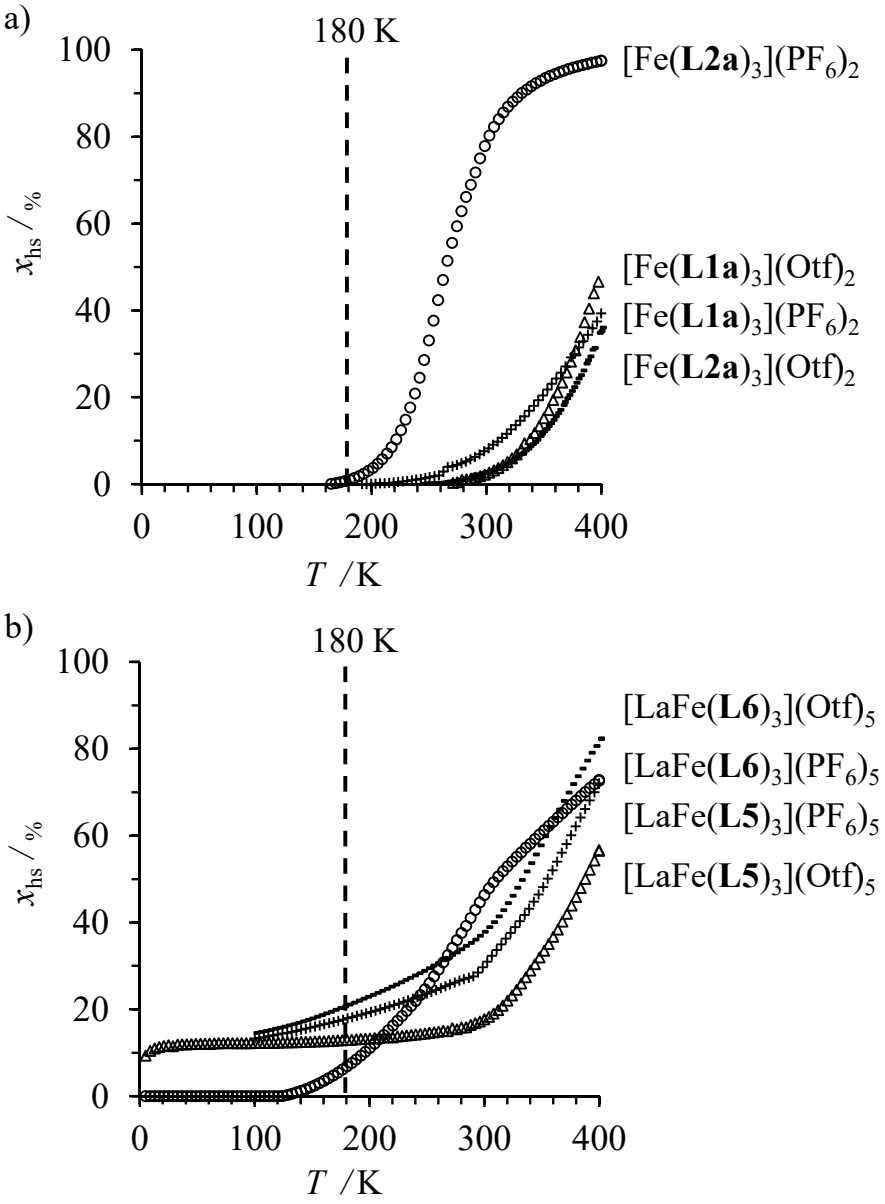

Figure S9. Mole fractions of high spin Fe^{II} versus *T* plot computed with Eq. (3) for a) mononuclear and b) dinuclear spin-crossover homoleptic tris-diimine Fe^{II} complexes (solid state, Otf^- = $CF_3SO_3^-$). The temperature at which the X-ray crystal structures has been measured is highlighted (180 K).

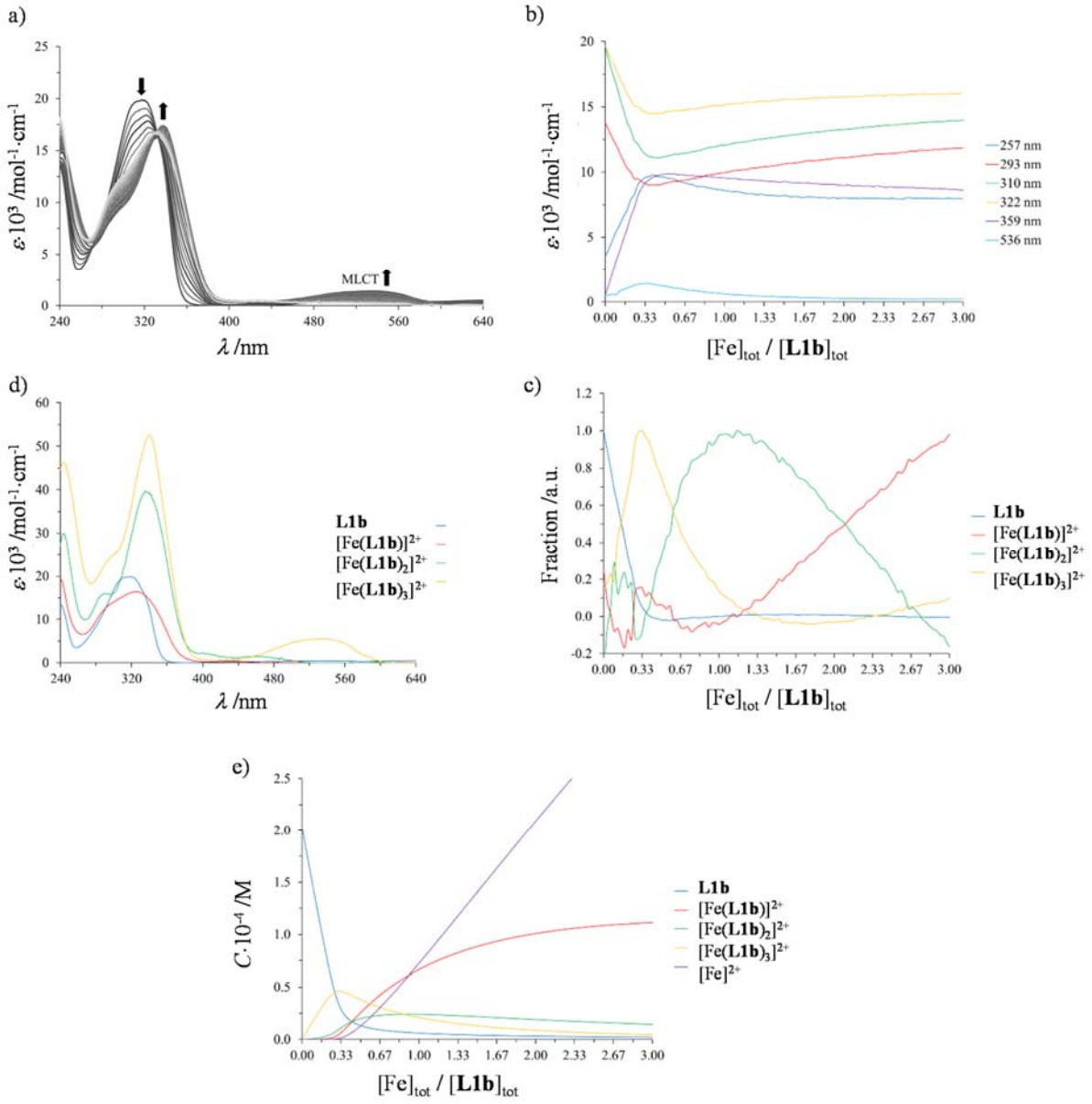

Figure S10. a) Variation of absorption spectra and b) corresponding variation of observed molar extinctions at different wavelengths recorded for the spectrophotometric titration of **L1b** with $Fe(CF_3SO_3)_2$ (total ligand concentration: $2.0 \cdot 10^{-4}$ mol·dm^{-3} in acetonitrile, 298 K). c) Evolving factor analysis using four absorbing eigenvectors,[21] d) re-constructed individual electronic absorption spectra,[22] and e) associated speciation.[TL1]

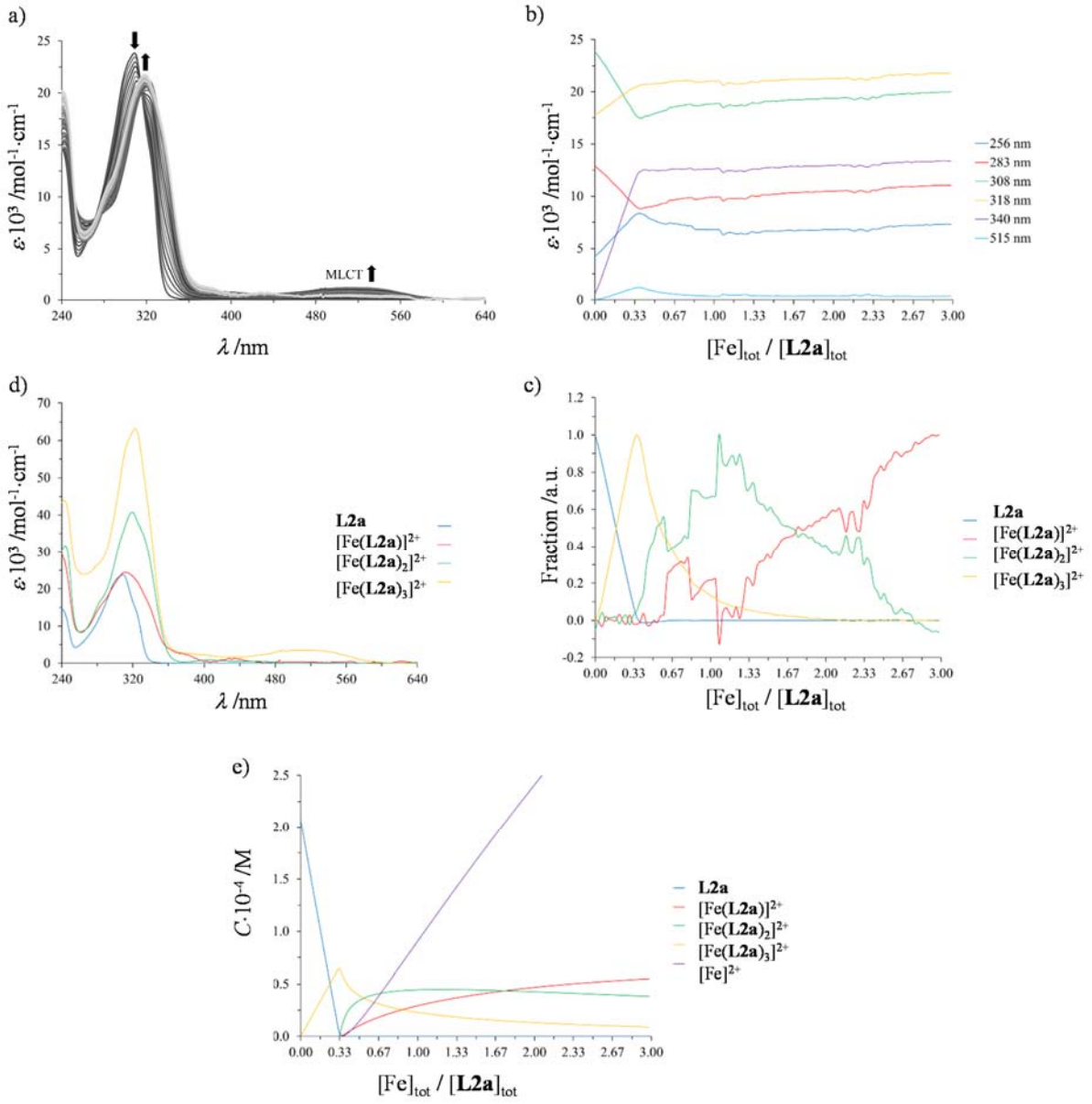

Figure S11. a) Variation of absorption spectra and b) corresponding variation of observed molar extinctions at different wavelengths recorded for the spectrophotometric titration of **L2a** with $Fe(CF_3SO_3)_2$ (total ligand concentration: $2.0 \cdot 10^{-4}$ mol·dm^{-3} in acetonitrile, 298 K). c) Evolving factor analysis using four absorbing eigenvectors,[21] d) re-constructed individual electronic absorption spectra,[22] and e) associated speciation.[TL1]

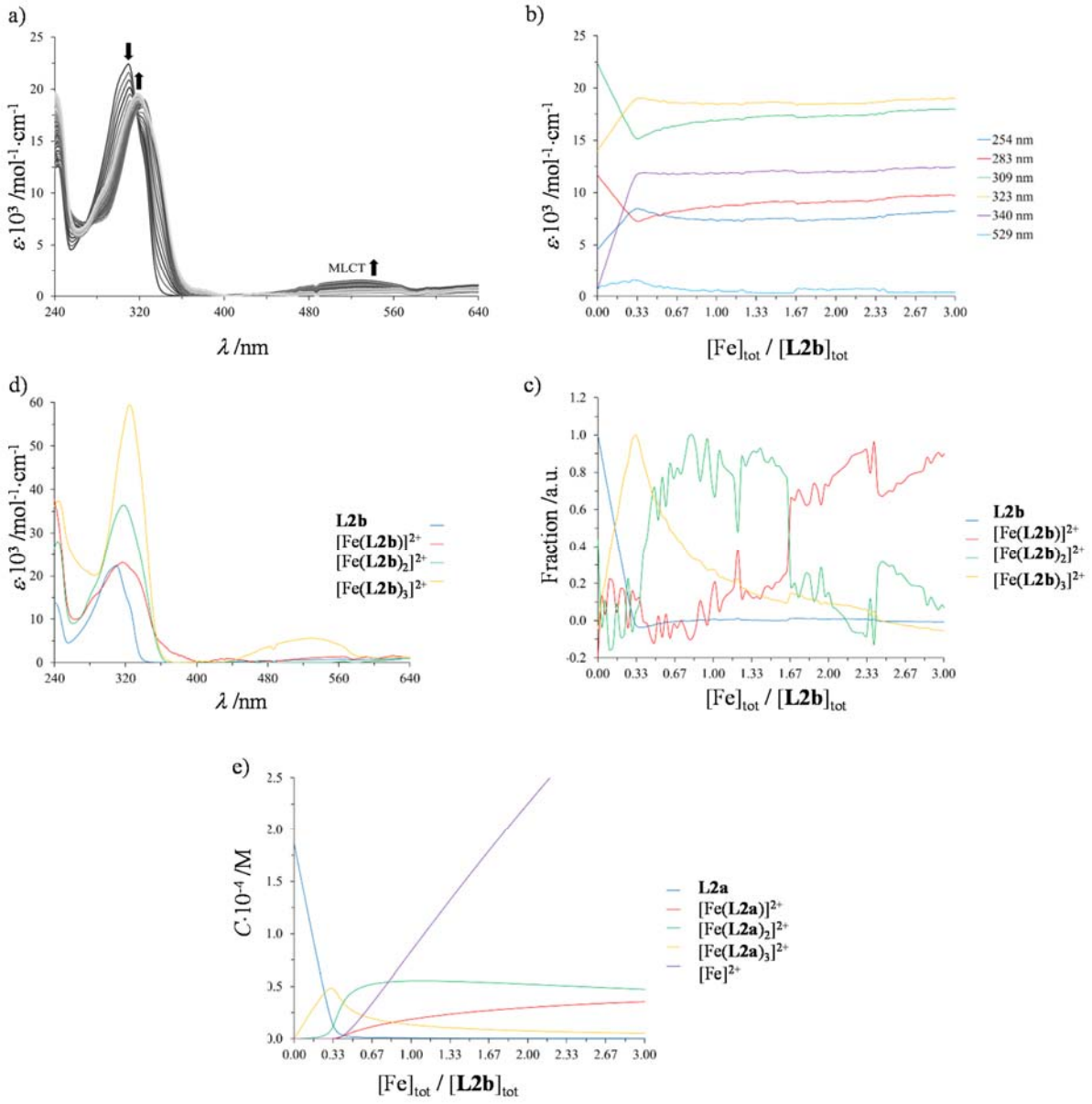

Figure S12. a) Variation of absorption spectra and b) corresponding variation of observed molar extinctions at different wavelengths recorded for the spectrophotometric titration of **L2b** with $Fe(CF_3SO_3)_2$ (total ligand concentration: $2.0 \cdot 10^{-4}$ mol·dm^{-3} in acetonitrile, 298 K). c) Evolving factor analysis using four absorbing eigenvectors,[21] d) re-constructed individual electronic absorption spectra,[22] and e) associated speciation.[TL1]

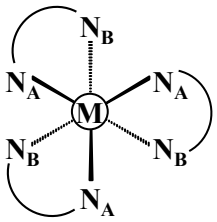

fac-$[Fe(\mathbf{L}\boldsymbol{k})_3]^{2+}$

$$\beta_{1,3,fac}^{Fe,\mathbf{L}\boldsymbol{k}} = 16\left(f^{Fe,\mathbf{L}\boldsymbol{k}}\right)^3\left(u_{cis,fac}^{\mathbf{L}\boldsymbol{k},\mathbf{L}\boldsymbol{k}}\right)^3 \quad (S1)$$

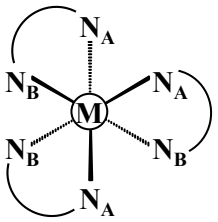

mer-$[Fe(\mathbf{L}\boldsymbol{k})_3]^{2+}$

$$\beta_{1,3,mer}^{Fe,\mathbf{L}\boldsymbol{k}} = 48\left(f^{Fe,\mathbf{L}\boldsymbol{k}}\right)^3\left(u_{cis,mer}^{\mathbf{L}\boldsymbol{k},\mathbf{L}\boldsymbol{k}}\right)^2 u_{cis,fac}^{\mathbf{L}\boldsymbol{k},\mathbf{L}\boldsymbol{k}} \quad (S2)$$

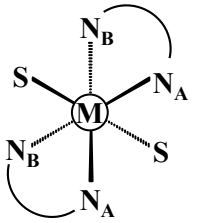

trans-fac-$[Fe(\mathbf{L}\boldsymbol{k})_2(CH_3CN)_2]^{2+}$

$$\beta_{1,2,trans-fac}^{Fe,\mathbf{L}\boldsymbol{k}} = 12\left(f^{Fe,\mathbf{L}\boldsymbol{k}}\right)^2 u_{trans,fac}^{\mathbf{L}\boldsymbol{k},\mathbf{L}\boldsymbol{k}} \quad (S3)$$

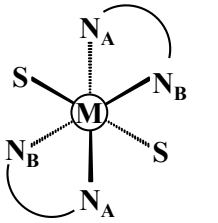

trans-mer-$[Fe(\mathbf{L}\boldsymbol{k})_2(CH_3CN)_2]^{2+}$

$$\beta_{1,2,trans-mer}^{Fe,\mathbf{L}\boldsymbol{k}} = 12\left(f^{Fe,\mathbf{L}\boldsymbol{k}}\right)^2 u_{trans,mer}^{\mathbf{L}\boldsymbol{k},\mathbf{L}\boldsymbol{k}} \quad (S4)$$

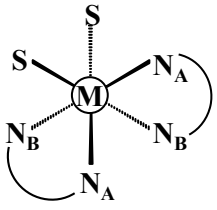

cis-fac-$[Fe(\mathbf{L}\boldsymbol{k})_2(CH_3CN)_2]^{2+}$

$$\beta_{1,2,cis-fac}^{Fe,\mathbf{L}\boldsymbol{k}} = 48\left(f^{Fe,\mathbf{L}\boldsymbol{k}}\right)^2 u_{cis,fac}^{\mathbf{L}\boldsymbol{k},\mathbf{L}\boldsymbol{k}} \quad (S5)$$

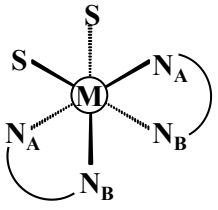

cis-merA-$[Fe(\mathbf{L}\boldsymbol{k})_2(CH_3CN)_2]^{2+}$

$$\beta_{1,2,cis-merA}^{Fe,\mathbf{L}\boldsymbol{k}} = 24\left(f^{Fe,\mathbf{L}\boldsymbol{k}}\right)^2 u_{cis,mer}^{\mathbf{L}\boldsymbol{k},\mathbf{L}\boldsymbol{k}} \quad (S6)$$

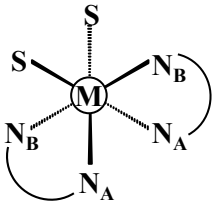

cis-merB-$[Fe(\mathbf{L}\boldsymbol{k})_2(CH_3CN)_2]^{2+}$

$$\beta_{1,2,cis-merB}^{Fe,\mathbf{L}\boldsymbol{k}} = 24\left(f^{Fe,\mathbf{L}\boldsymbol{k}}\right)^2 u_{cis,mer}^{\mathbf{L}\boldsymbol{k},\mathbf{L}\boldsymbol{k}} \quad (S7)$$

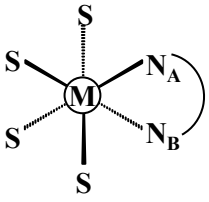

$[Fe(\mathbf{L}\boldsymbol{k})(CH_3CN)_4]^{2+}$

$$\beta_{1,1}^{Fe,\mathbf{L}\boldsymbol{k}} = 24 f^{Fe,\mathbf{L}\boldsymbol{k}} \quad (S8)$$

Figure S13. Microspecies and associated microscopic formation constants considered for the complexes $[Fe(\mathbf{L}\boldsymbol{k})_3]^{2+}$ (Eqs S1-S2), $[Fe(\mathbf{L}\boldsymbol{k})_2(CH_3CN)_2]^{2+}$ (Eqs S3-S7) and $[Fe(\mathbf{L}\boldsymbol{k})(CH_3CN)_4]^{2+}$ (Eq. S8). For $[Fe(\mathbf{L}\boldsymbol{k})_2(CH_3CN)_2]^{2+}$, The *cis*/*trans* terminology is used for describing the relative orientation of the two solvent molecules, whereas the additional *mer*/*fac* designation refers to the relative orientation of the two unsymmetrical didentate ligands as defined in the saturated $[Fe(\mathbf{L}\boldsymbol{k})_3]^{2+}$ complex. A *trans* N_A-Fe-N_A arrangement is therefore noted as *merA*, a *trans* N_B-Fe-N_B is noted as *merB* and a *trans* N_A-Fe-N_B is noted *fac.*

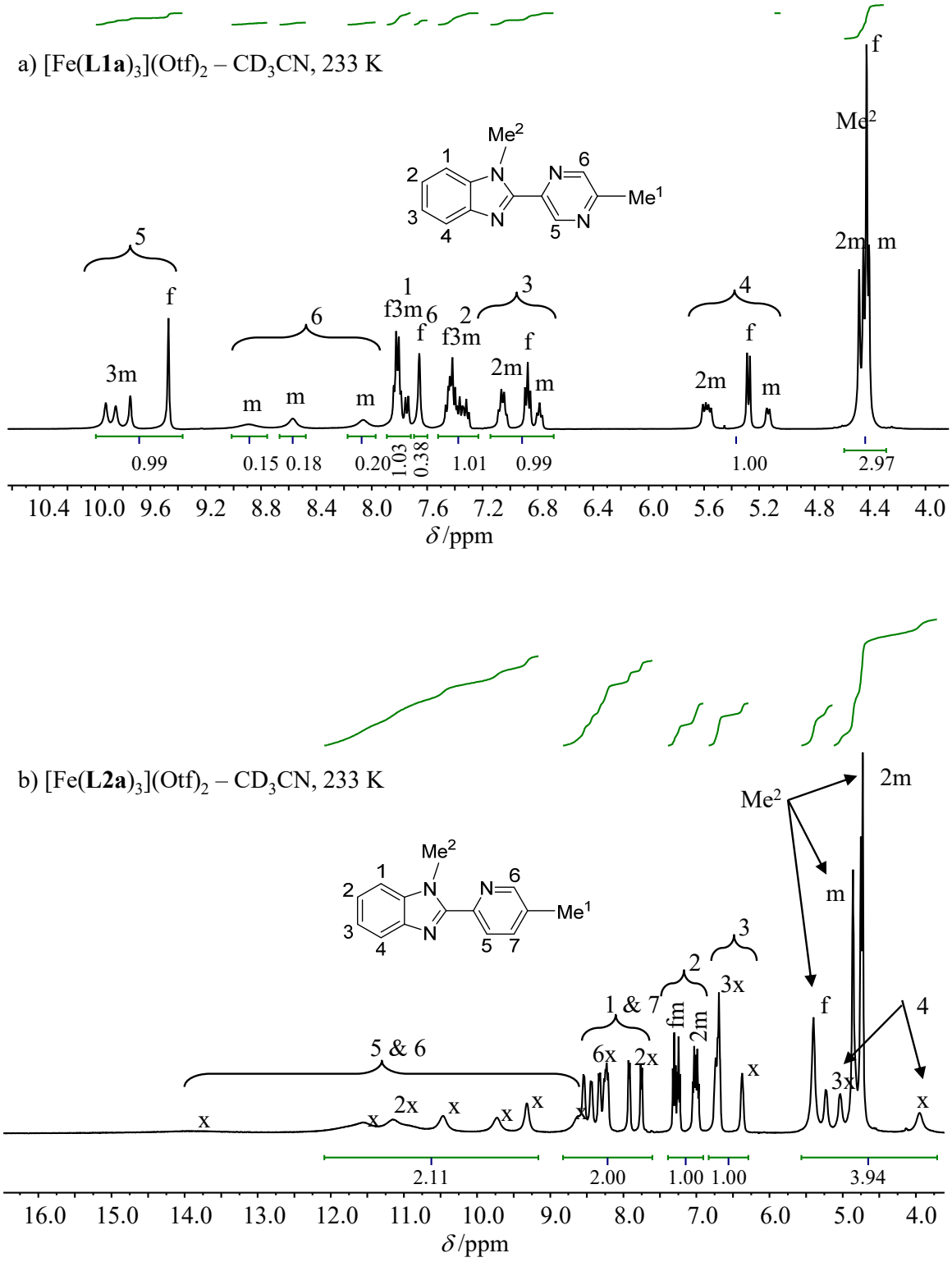

Figure S14. ^{1}H NMR spectra of a) [Fe(**L1a**)$_3$]$^{2+}$ and b) [Fe(**L2a**)$_3$]$^{2+}$ with assignment recorded in CD$_3$CN at 233 K (f = *fac*, m = *mer*, x = *fac* or *mer*). The signals for Me^1 are not shown.

a) [Fe(**L1a**)$_3$](CF$_3$SO$_3$)$_2$

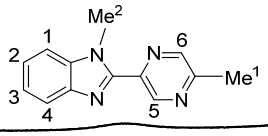

b) [Fe(**L2a**)$_3$](CF$_3$SO$_3$)$_2$

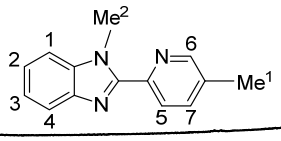

Figure S15. ^{1}H NMR spectra of a) [Fe(**L1a**)$_3$]$^{2+}$ and b) [Fe(**L2a**)$_3$]$^{2+}$ with assignment recorded in CD_3CN at variable temperatures (f = *fac*, m = *mer*, x = *fac* or *mer*. The red rectangles highlight the signals used for estimating $K_{iso}^{mer \rightarrow fac}$.

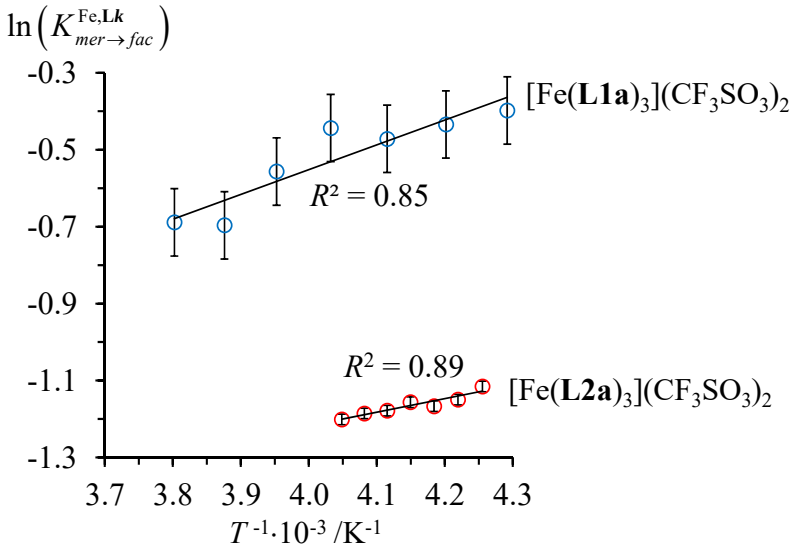

Figure S16. Van't Hoff plots pertinent to equilibrium (10) for a) [Fe(**L1a**)$_3$]$^{2+}$ and b) [Fe(**L2a**)$_3$]$^{2+}$ in CD_3CN.

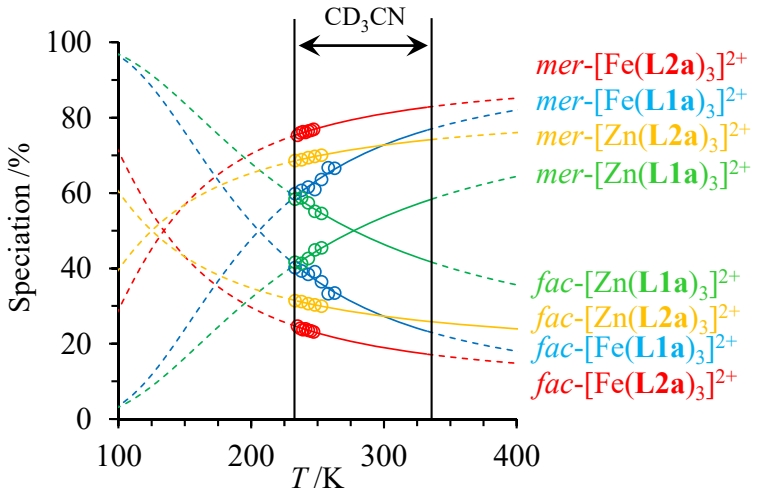

Figure S17. Speciation of *fac*-[M(**L*k***)$_3$]$^{2+}$ and *mer*-[M(**L*k***)$_3$]$^{2+}$ in CD_3CN (M = Fe^{II}, Zn^{II} and **L*k*** = **L1a**, **L2a**). Dots = experimental points, full traces = simulation in the 233-333 K range compatible with CD_3CN and doted traces = extrapolation outside the accessible temperature range in CD_3CN.

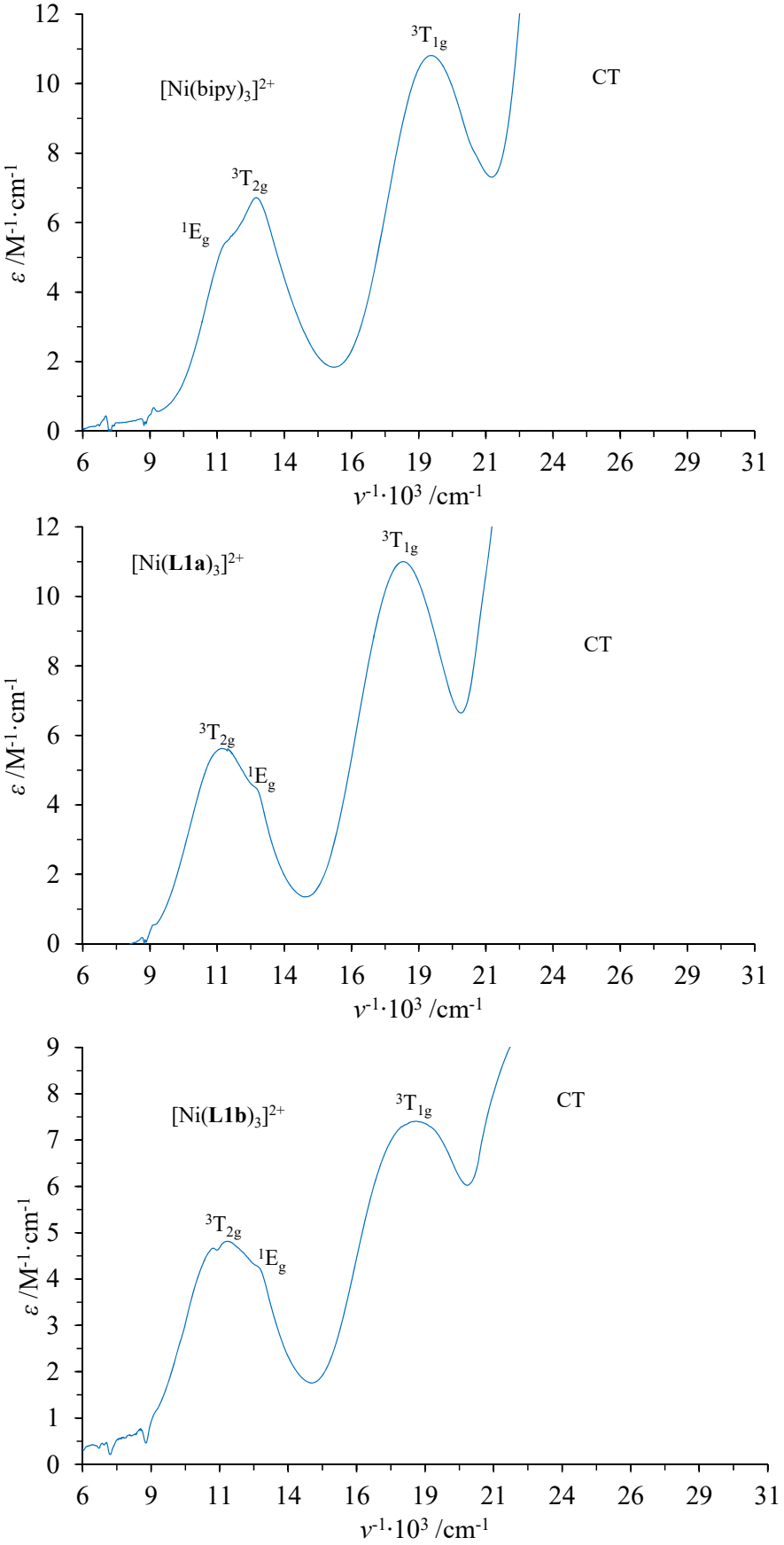
[Ni(bipy)3]2+
3T1g
3T2g
1Eg
CT
ε /M-1·cm-1
ν-1·103 /cm-1
[Ni(L1a)3]2+
3T1g
3T2g
1Eg
CT
ε /M-1·cm-1
ν-1·103 /cm-1
[Ni(L1b)3]2+
3T1g
3T2g
1Eg
CT
ε /M-1·cm-1
ν-1·103 /cm-1

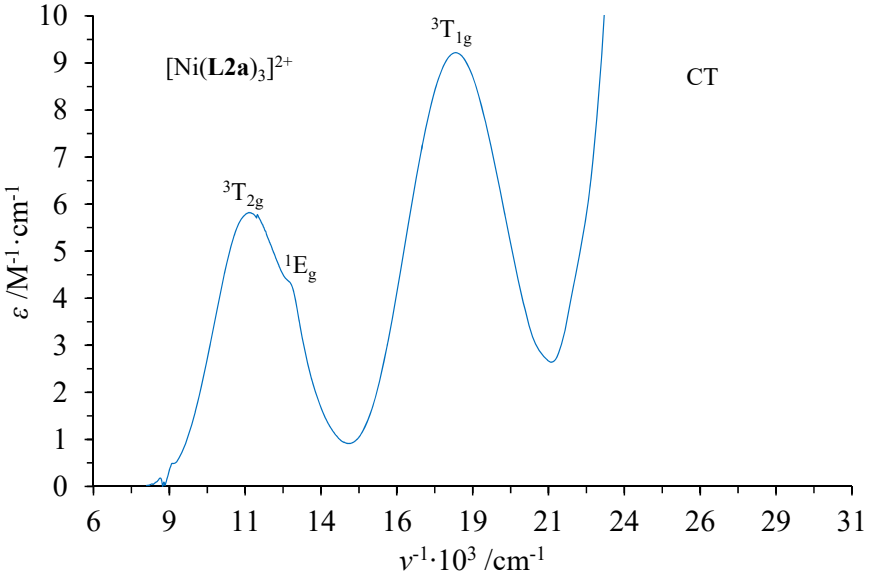
[Ni(L2a)3]2+
3T1g
3T2g
1Eg
CT
ε /M-1·cm-1
ν-1·103 /cm-1

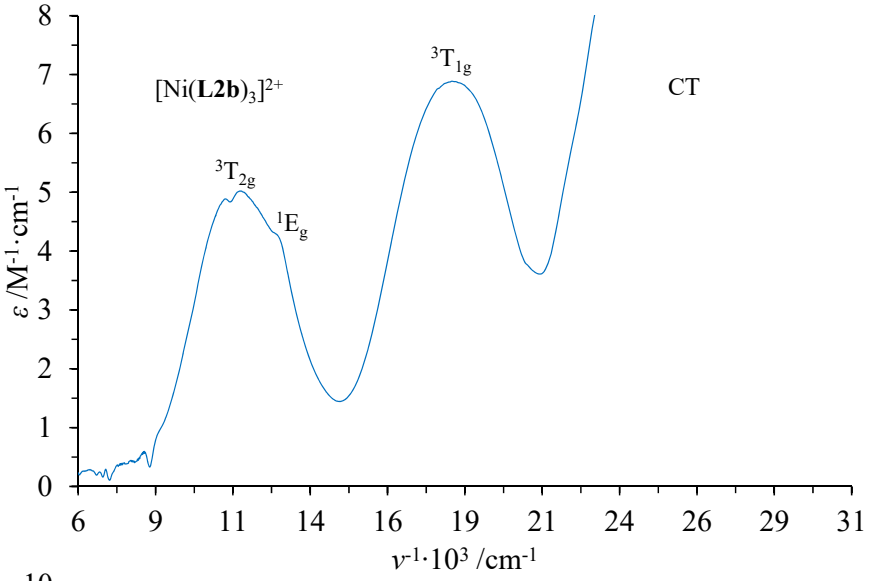
[Ni(L2b)3]2+
3T1g
3T2g
1Eg
CT
ε /M-1·cm-1
ν-1·103 /cm-1

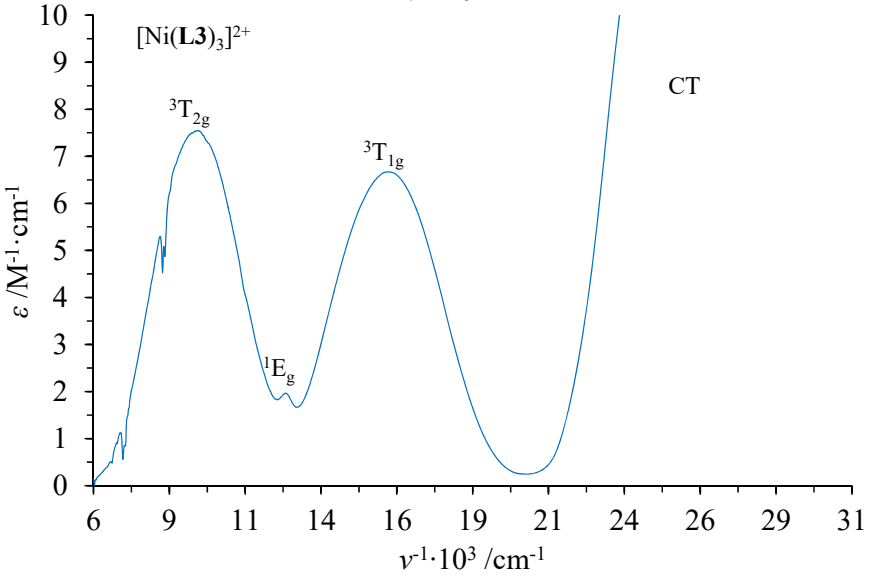
[Ni(L3)3]2+
3T2g
3T1g
1Eg
CT
ε /M-1·cm-1
ν-1·103 /cm-1

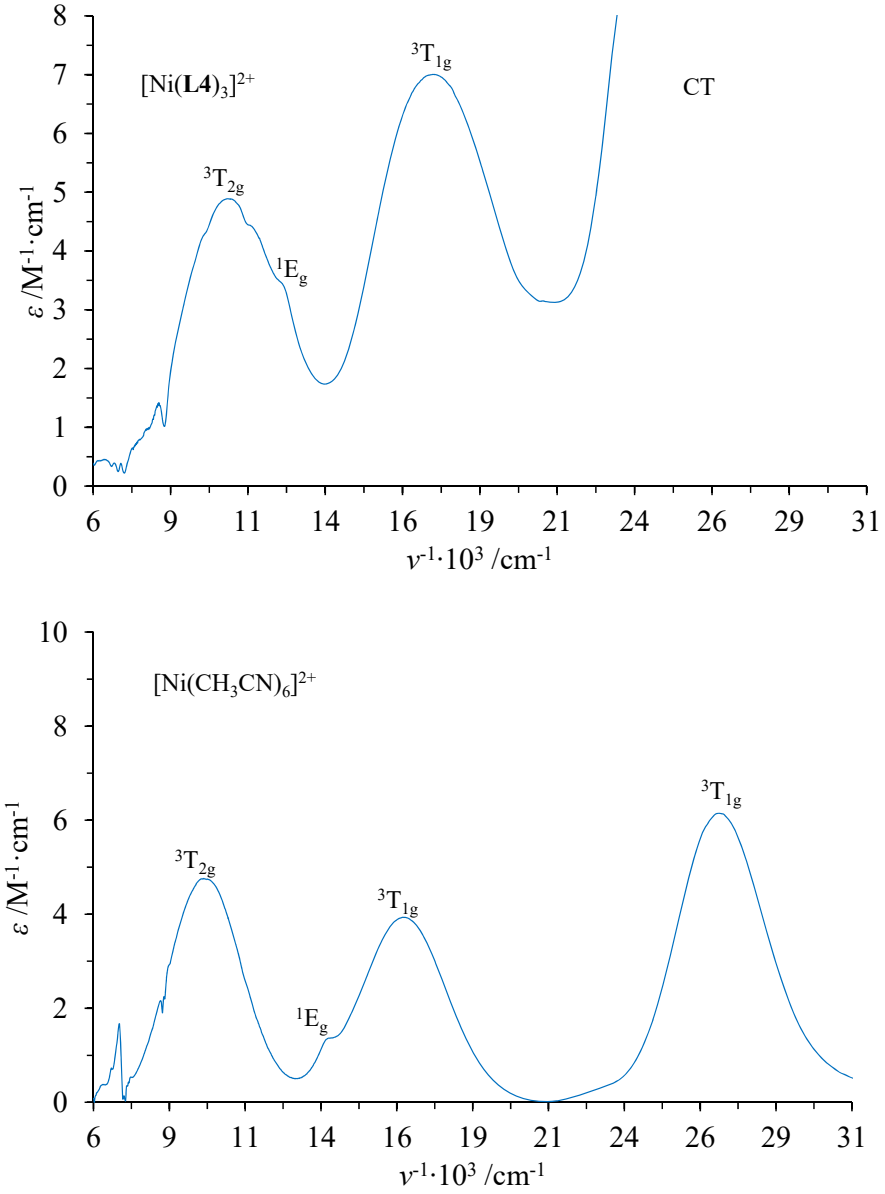

Figure S18. Absorption spectra of $[Ni(\mathbf{L}\boldsymbol{k})_3]^{2+}$ complexes (0.1 M in acetonitrile, 293 K).

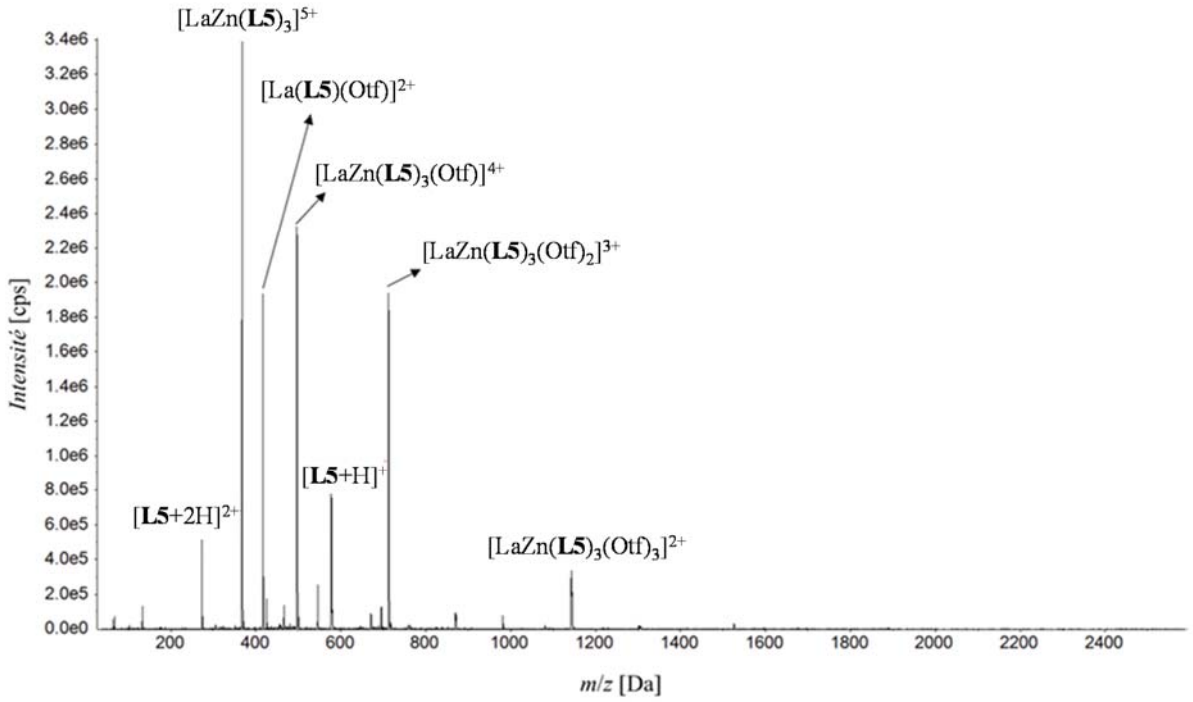

Figure S19. ESI-MS (soft-positive) mass spectrum of $[LaZn(\mathbf{L5})_3](OTf)_5$ ($2\cdot10^{-3}$ M in CH_3CN, 298 K).

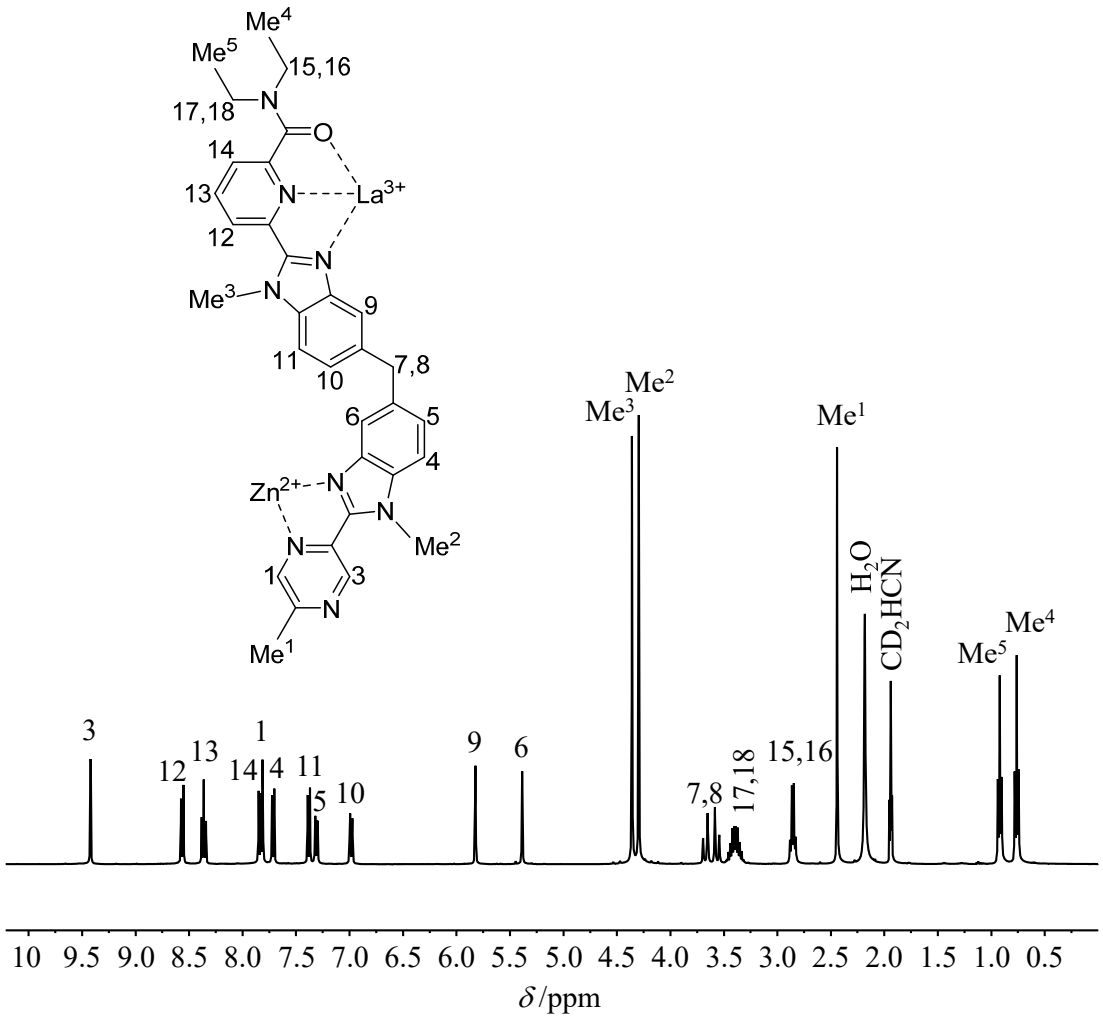

Figure S20. ^{1}H NMR spectrum of [LaZn(**L5**)$_3$](Otf)$_5$ ($2\cdot10^{-3}$ M in CD_3CN, 293 K).

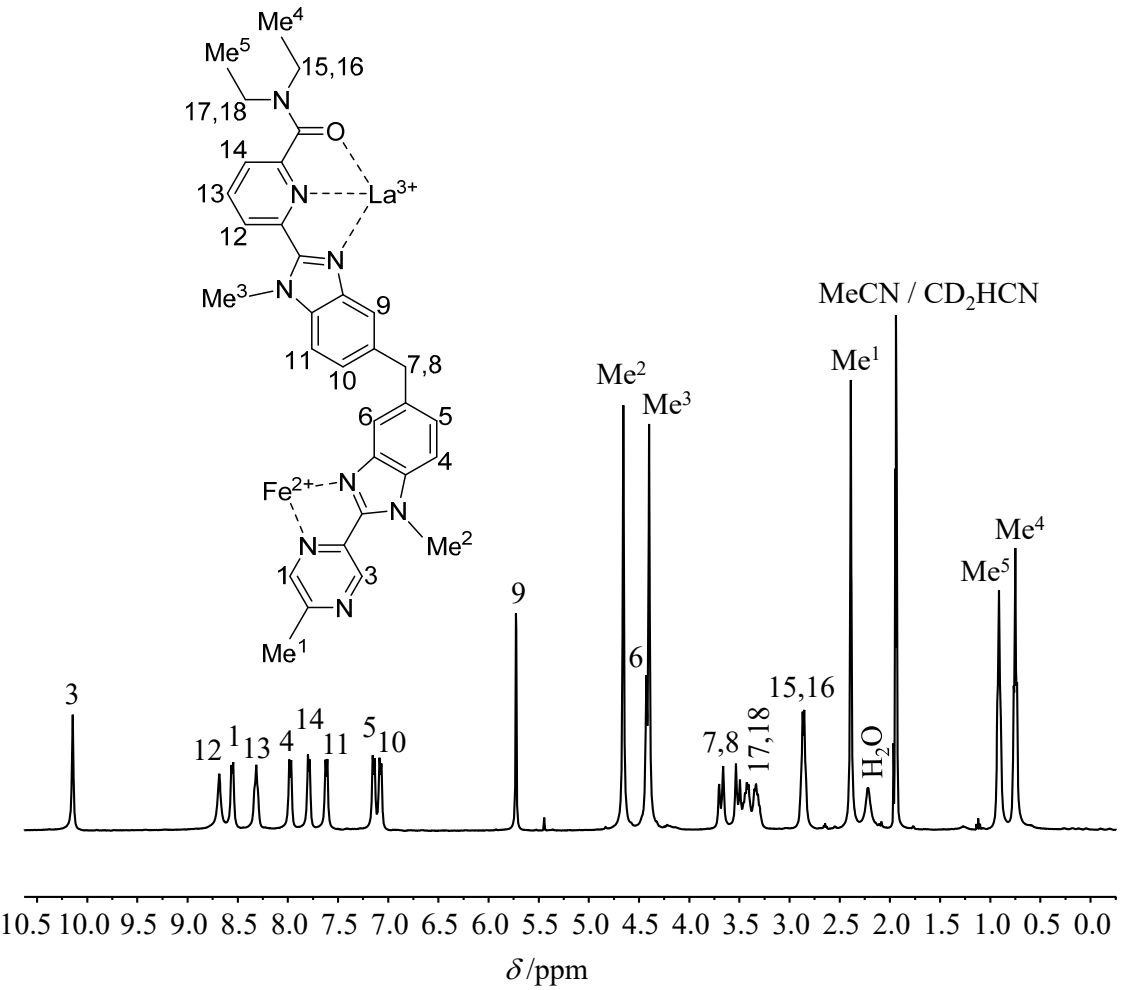

Figure S21. ^{1}H NMR spectrum of [LaFe(**L5**)$_3$](Otf)$_5$ ($2\cdot10^{-3}$ M in CD_3CN, 293 K).

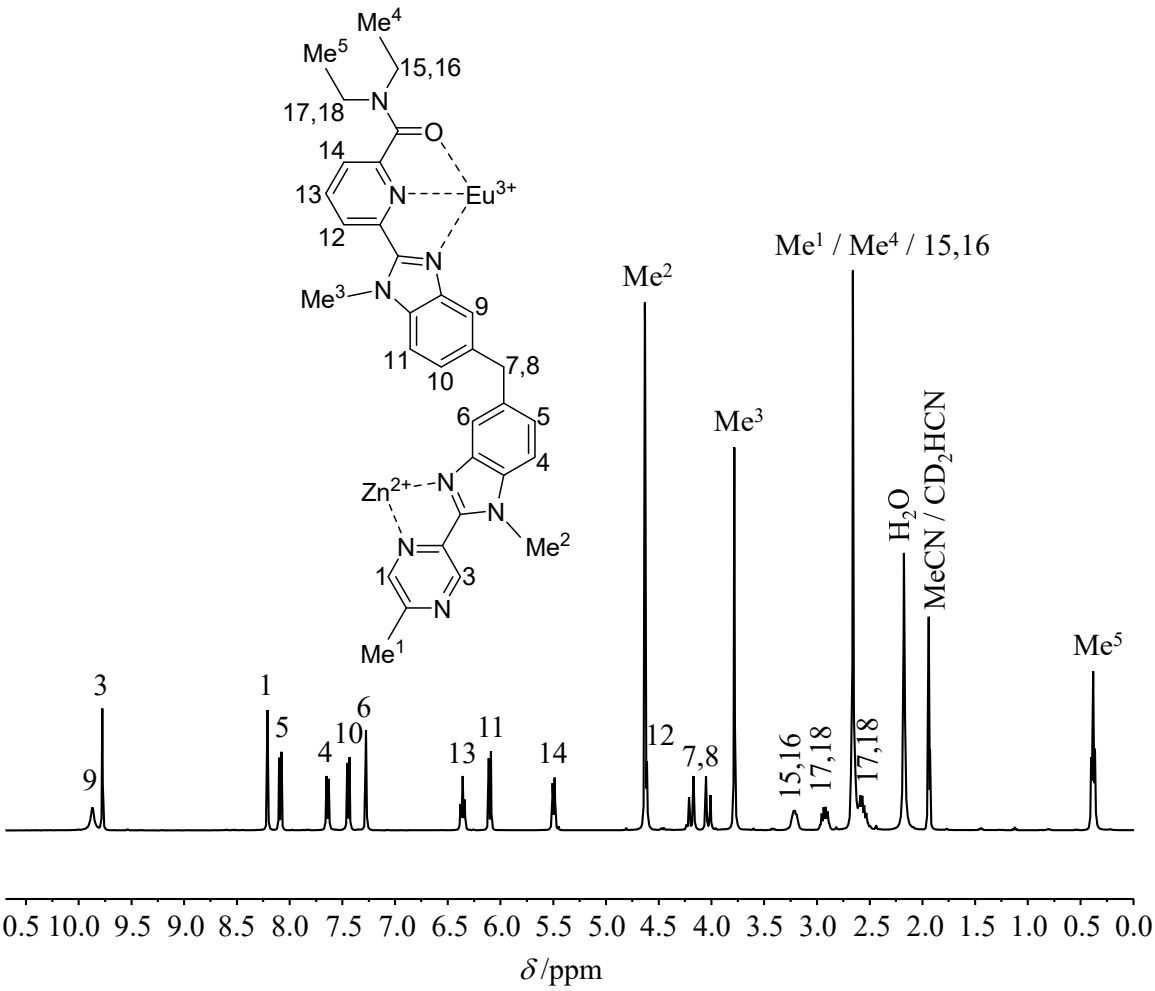

Figure S22. ^{1}H NMR spectrum of [EuZn(**L5**)$_3$](Otf)$_5$ ($2\cdot10^{-3}$ M in CD_3CN, 293 K).

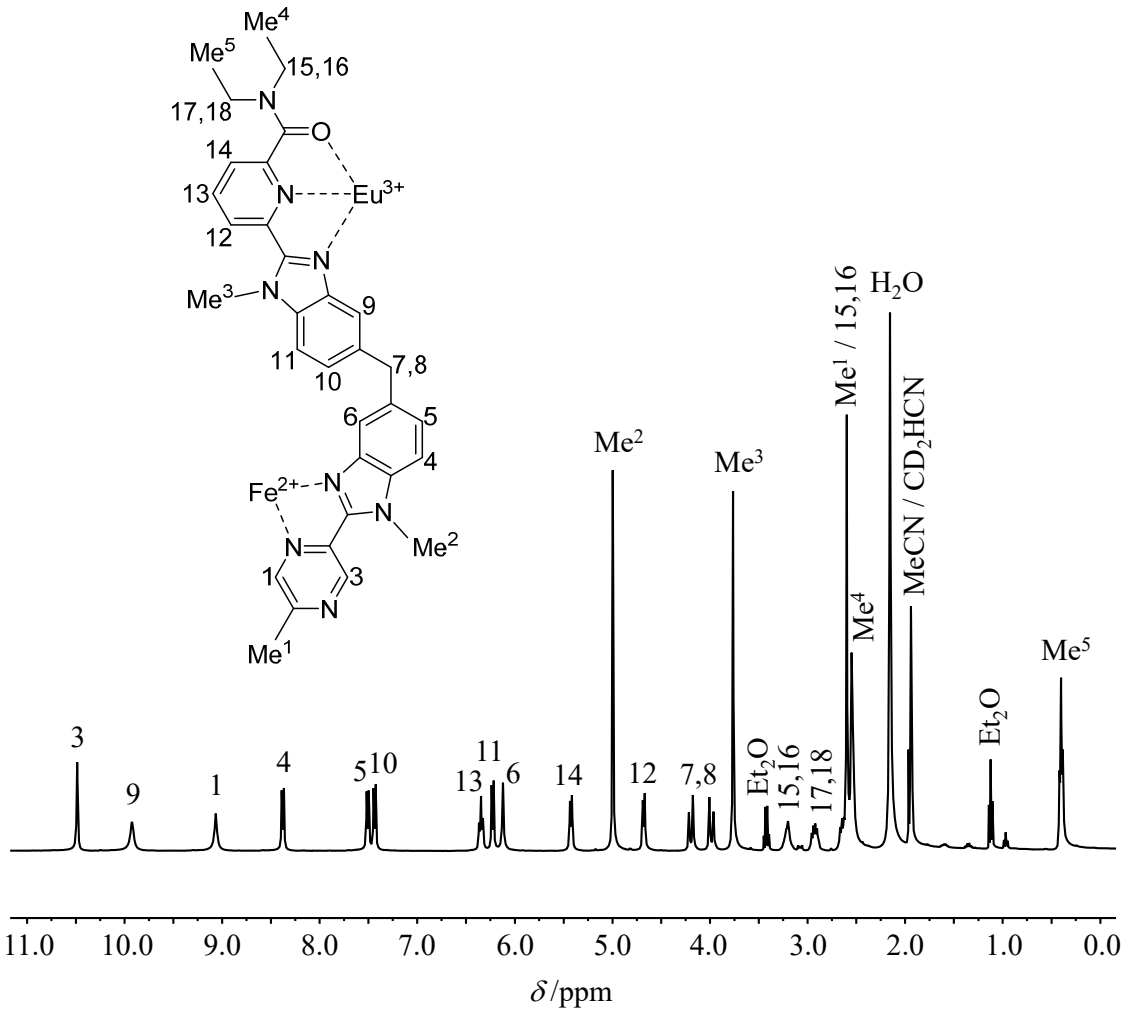

Figure S23. ^{1}H NMR spectrum of [EuFe(**L5**)$_3$](Otf)$_5$ (2·10^{-3} M in CD_3CN, 293 K).

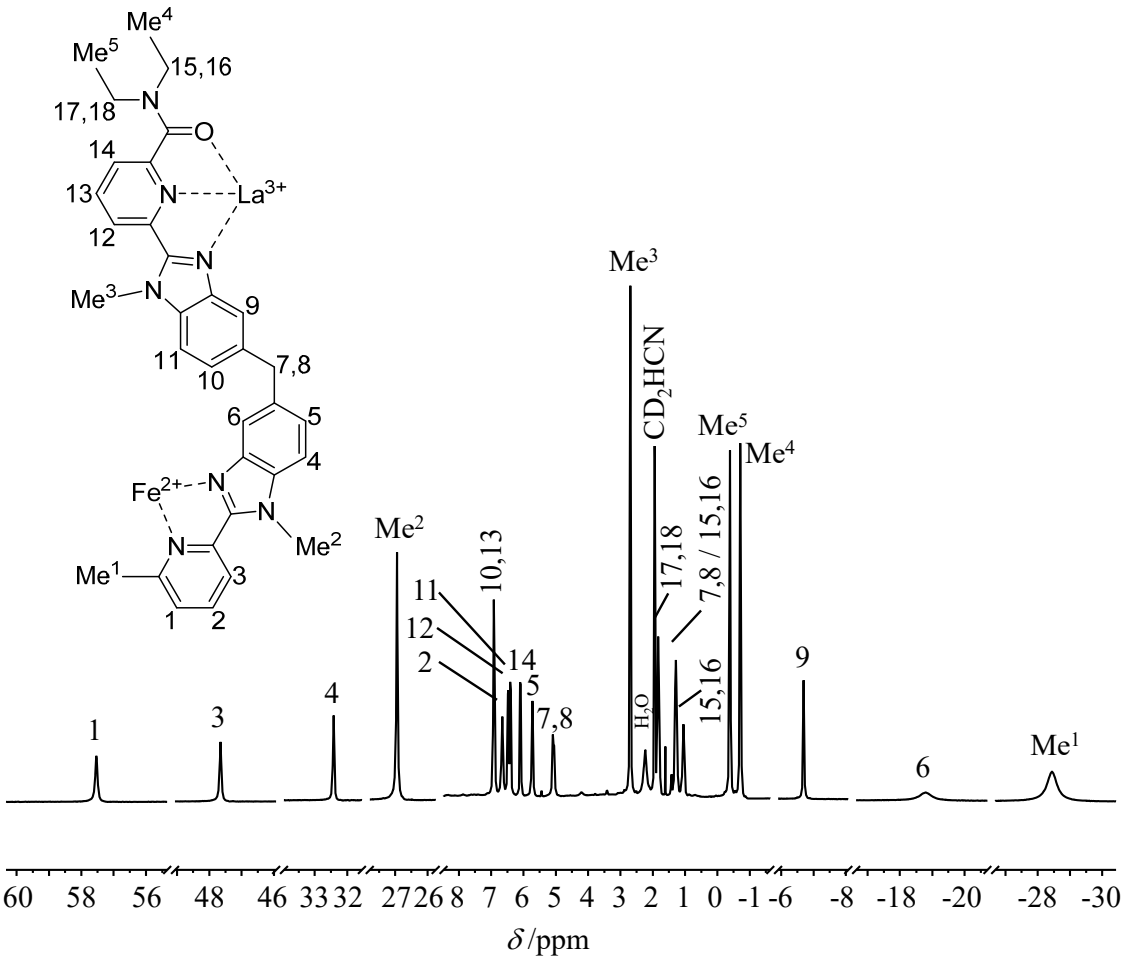

Figure S24. ^{1}H NMR spectrum of [LaFe(**L7**)$_3$](Otf)$_5$ (2·10^{-3} M in CD_3CN, 293 K).

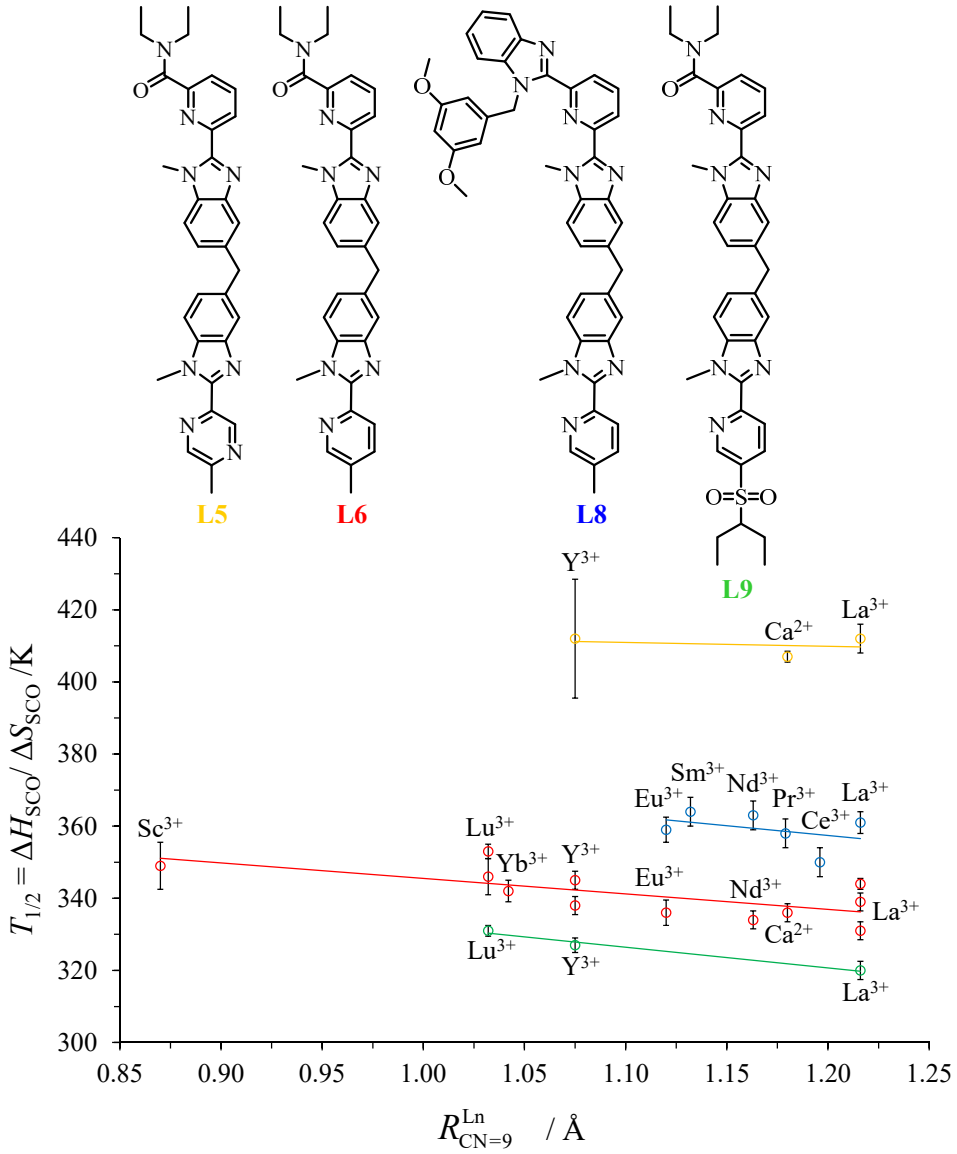

Figure S25. SCO transition temperatures $T_{1/2}$ measured for triple-stranded *HHH*-[LnFe(**L*k***)$_3$]$^{5+}$ along the lanthanide series (CD_3CN).[18b][49d],[56] $R^{Ln}_{CN=9}$ are the ionic radius of nine-coordinate trivalent lanthanide cations.